Title
THE NUCLEAR SEYLER-BLANCHARD MODEL IN THE HARTREE APPROXIMATION

Author
Randrup, J.

Publication Date
1974-09-01

Submitted to
Nuclear Physics A

LBL-3413
Preprint c.2

THE NUCLEAR SEYLER-BLANCHARD MODEL IN THE HARTREE APPROXIMATION

J. Randrup

September 1974

Prepared for the U. S. Atomic Energy Commission
under Contract W-7405-ENG-48

LBL-3413
c.2

DISCLAIMER

THE NUCLEAR SEYLER-BLANCHARD MODEL IN THE HARTREE APPROXIMATION*

J. Randrup†

Lawrence Berkeley Laboratory
University of California
Berkeley, California 94720

December 1974

ABSTRACT

The model for macroscopic nuclear properties introduced by Seyler and Blanchard within the framework of the Thomas-Fermi approximation is developed in the Hartree approximation. The quantization of the velocity-dependent two-nucleon interaction is discussed, and the general expressions for the interaction-energy density and the effective single-particle Hamiltonian are established. The developed model is applied to semi-infinite symmetric nuclear matter and comparison is made with the Thomas-Fermi results.

---

*Work done under the auspices of the U. S. Atomic Energy Commission.

†On leave from the University of Aarhus, Aarhus, Denmark.

CONTENTS

1. INTRODUCTION

The nuclear model introduced by Seyler and Blanchard[1] in 1961 has proved a very useful tool for the study of macroscopic properties of nuclei. The model is based on a simple phenomenological two-nucleon interaction (often referred to as the Seyler-Blanchard interaction), having the following form,

$$V_{12} = -Cg\left(\frac{r_{12}}{a}\right)\left(1 - p_{12}^2/b^2\right) \quad , \quad g(r) = \frac{e^{-r}}{r} \tag{1.1}$$

Here r_{12} is the distance between the two interacting nuclei and $\vec{p}_{12} = \vec{p}_1 - \vec{p}_2$ their relative momentum. Thus the spatial part of the Seyler-Blanchard interaction is a Yukawa function of range a. The interaction strength C depends on whether the two nucleons are 'like' (i.e., two neutrons or two protons) or 'unlike' (i.e., a neutron and a proton). In addition, the strength of the interaction depends on the relative momentum p_{12} of the two nucleons; it becomes weaker as p_{12} increases and for some value b (the 'saturation' momentum) it changes from attractive to repulsive.

The momentum-dependent part of the Seyler-Blanchard interaction imitates the effect of a repulsive core in the two-nucleon potential and is responsible for the production of a nuclear saturation. The interaction seems to account reasonably well for the low-energy part of the effective nucleon-nucleus interaction inferred from experiment.

Only a few input parameters enter into the model: the Yukawa range a, the saturation momentum b, and the interactions strengths C_ℓ and C_u pertaining to like and unlike nucleon pairs, respectively. They may be determined from the experimentally known values of the nuclear radius

constant r_0, the volume-energy coefficient a_v, the surface-energy coefficient a_s, and the symmetry-energy coefficient J.

The fact that one wishes to extract information about the *macroscopic* nuclear properties only, permits the use of relatively simple approximations for the treatment of the associated many-body problem. Up to now, the model has been studied almost exclusively within the Thomas-Fermi approximation. This approximation leads to a very simple description of the nuclear system.

Seyler and Blanchard showed[1] that in this way it was possible to reproduce the gross nuclear energetics and sizes given by experiment, for reasonable values of the few input parameters. Later on, Myers and Swiatecki[2] adapted the model for their systematic study of macroscopic properties of nuclei and they employed the model for the calculation of the preliminary set of Droplet-Model coefficients. Furthermore, the model has been used as a basis for studying the thermostatic properties of nuclear matter.[3] Recently it has been used for the estimation of the nuclear 'proximity' force.[4] Presently, work[5,6] is being planned to further employ the model in the study of static as well as dynamical aspects of nucleus-nucleus collision processes.

The Seyler-Blanchard model, in its Thomas-Fermi formulation, has thus a wide range of applicability, and because of its great mathematical simplicity it is a very helpful tool for the study of macroscopic nuclear properties. It is obvious, however, that in the nuclear surface region, where the potential varies rapidly, the Thomas-Fermi approximation is rather crude as it neglects the phase correlations imposed by the surface as well as the penetration of particles into the classically forbidden

region. Considering the great virtue of the model, it would be very valuable to clarify, in a quantitative way, how much a more proper treatment of the quantum-mechanics would affect the results.

In this paper we study the Seyler-Blanchard model within the Hartree approximation. At the same time we formulate the model in more general terms so that it applies also to the general situation of non-static systems. The Hartree approximation treats the quantum-mechanics in an exact way, within the restriction that the many-particle system be described by a product wave function. Like the Thomas-Fermi approximation, the Hartree approximation neglects effects associated with the correlation between individual particles, and it constitutes a natural basis for studying the macroscopic properties of a quantum system. Let us stress at this point that the aim is not to develop a realistic microscopic model for real nuclei, but rather to establish a conceptually simple model from which the average behavior of nuclear matter may be inferred. In so doing we are concerned with the macroscopic limit of a large particle number so that individual-particle effects may be neglected.

The development of the Seyler-Blanchard model in the Hartree approximation provides us with a possibility for determining the accuracy of the Thomas-Fermi approximation for nuclear matter. Moreover, it makes it possible to obtain more accurate values for the various macroscopic nuclear properties, as for example, those represented by the Droplet-Model coefficients.[2]

In addition to thus yielding a more detailed insight into the properties of isolated static nuclear systems, the development of the model presented here has importance for more general situations encountered,

for example that of two colliding nuclei.

The paper is structured as follows. First we take the effort to clarify the notational framework and general formalism with which we shall tackle the problem. We find this worthwhile in order to make the later presentation easy and transparent. After this, we analyze in some detail the problems associated with the quantum representation of the momentum-dependent term of the interaction. With this problem settled, we then proceed to develop the general formulae of the model. As an illustration, the model is then applied to semi-infinite symmetric nuclear matter. Finally, we present a summary of the investigation together with a discussion of various prospects. We have added an Appendix for an outline of the numerical aspects of the semi-infinite problem.

2. FORMALISM

We shall start out by describing the general formalism in terms of which we shall develop the quantum-mechanical formulation of the model. A clarification of the various definitions and concepts at this early point will ease the presentation later on and, moreover, may serve as a basis for future reference.

In this work we are concerned with a many-nucleon system which may be described well in terms of independent-particle motion. Since the nucleons are fermions, the proper type of wave function is an anti-symmetrical product of single-particle wave functions (a Slater determinant),

$$\Psi_{\nu_1\nu_2\ldots\nu_A}(\xi_1,\xi_2,\ldots,\xi_A)_a = \mathcal{A}\psi_{\nu_1}(\xi_1)\psi_{\nu_2}(\xi_2)\ldots\psi_{\nu_A}(\xi_A) \tag{2.1}$$

Here the quantum numbers ν_i are a complete set of labels for the occupied

one-particle orbits, and the coordinates of a particle i (its position $\vec{r}_i$ together with its spin and isospin variables) are denoted by ξ_i. This notation is in accordance with ref. 7. Furthermore, $\mathcal{A}$ is the anti-symmetrization operator, which transforms a product wave function into the the corresponding Slater determinant.

2.1. Density Distributions

The macroscopic system properties we are interested in for our present study (the matter distribution, the energy distribution, etc.) are given in terms of one-point density distributions $\alpha(\vec{r})$ depending on one spatial point $\vec{r}$. In quantum mechanics, a density distribution $\alpha(\vec{r})$ to which we ascribe a physical reality is represented by a Hermitean density operator $\hat{\alpha}(\vec{r})$. (The symbol $\hat{}$ is employed to indicate an operator.) The density operator $\hat{\alpha}(\vec{r})$ representing a one-point density distribution acts on the individual particles separately and thus belong to the general category of one-particle operators.

In general, for a system of identical particles, a one-particle operator $\hat{F}$ has the form

$$\hat{F} = \sum_i \hat{F}(\xi_i) = \sum_i \hat{F}_i \qquad (2.2)$$

The last relation introduces the brief notation $\hat{F}_i$ for the term of the operator $\hat{F}$ referring to the coordinates of particle i. For a one-particle operator $\hat{F}$, the expectation value F in a many-particle state Ψ is given in terms of one-particle expectation values:

(2.3)

$$F \equiv \langle \hat{F} \rangle_\Psi = \sum_i \langle \nu_i | \hat{F} | \nu_i \rangle = \sum_i \langle \hat{F}_i \rangle_i \quad . \tag{2.3}$$

Here the brief notation $\langle \hat{F}_i \rangle_i$ denotes the expectation value of $\hat{F}(\xi_i)$ in the single-particle state $|\nu_i\rangle$. Thus the anti-symmetrization does not affect the expectation value (or, in general, the matrix elements) of a one-particle operator.

We may now proceed to introduce a number of density operators which will be helpful for the subsequent analysis of the Seyler-Blanchard interaction.

For convenience, we shall define the densities such that they all have the same dimension, namely inverse volume.

First, let us introduce the one-particle operator $\hat{\rho}$ representing the matter density distribution ρ. According to our remarks above, it is sufficient to specify the part $\hat{\rho}_i$. It is given by

$$\hat{\rho}_i(\vec{r}) = \delta(\vec{r} - \vec{r}_i) \tag{2.4}$$

It is important here to distinguish between the particle coordinate $\vec{r}_i$ and the spatial variable $\vec{r}$ which plays the role of a parameter entering in the operator. Thus the total matter density ρ is given by

$$\begin{aligned} \rho(\vec{r}) &= \sum_i \langle \hat{\rho}_i(\vec{r}) \rangle_i \\ &= \sum_i \int \psi^*_{\nu_i}(\vec{r}_i)\ \delta(\vec{r} - \vec{r}_i)\ \psi_{\nu_i}(\vec{r}_i) d^3\vec{r}_i \\ &= \sum_i \psi^*_{\nu_i}(\vec{r})\ \psi_{\nu_i}(\vec{r}) \end{aligned} \tag{2.5}$$

A second basic physical density distribution is the momentum density $\vec{\pi}$ which is represented by the operators

$$\hat{\vec{\pi}}_i(\vec{r}) = \frac{1}{2}\left\{\frac{\vec{p}_i}{b}, \hat{\rho}_i(\vec{r})\right\}$$

$$= \frac{1}{2}\left(\frac{\vec{p}_i}{b}\delta(\vec{r} - \vec{r}_i) + \delta(\vec{r} - \vec{r}_i)\frac{\vec{p}_i}{b}\right)$$

$$= \frac{1}{2}\left(\hat{\vec{\pi}}_i^+(\vec{r}) + \hat{\vec{\pi}}_i^-(\vec{r})\right) \qquad (2.6)$$

Here, of course, $\vec{p}_i$ denotes the momentum operator for particle i, $\vec{p}_i = -i\hbar\vec{\nabla}_i$; as no confusion can occur we omit the symbol $\hat{}$ over $\vec{p}_i$. Furthermore, we have used the anti-commutator construction $\{a,b\} \equiv ab + ba$ to ensure that the operator is Hermitean as it should be because it represents a physical quantity. The last relation indicates that the total momentum $\vec{\pi}(\vec{r})$ is composed at two parts $\vec{\pi}^+(\vec{r})$ and $\vec{\pi}^-(\vec{r})$, each of which is not Hermitean. For example, for a standing wave $\vec{\pi}^+$ is positive imaginary and $\vec{\pi}^-$ equally negative imaginary (which ensures the total momentum associated with a standing wave to be zero). It is important to point out that only the total momentum density $\vec{\pi} = \frac{1}{2}(\vec{\pi}^+ + \vec{\pi}^-)$ is physically meaningful and can have experimental significance. Notice that $\vec{\pi}$ measures the momentum density in units of b, the Seyler-Blanchard saturation momentum.

Thirdly, we shall define the operator $\hat{\tau}$ representing the kinetic energy density τ in the system,

$$\hat{\tau}_i(\vec{r}) = \frac{1}{2}\left\{\frac{p_i^2}{2m}, \hat{\rho}_i(\vec{r}) \quad \frac{2m}{b^2}\right\}$$

$$= \frac{1}{2}\left(\left(\frac{\vec{p}_i}{b}\right)^2 \delta(\vec{r} - \vec{r}_i) + \delta(\vec{r} - \vec{r}_i)\left(\frac{\vec{p}_i}{b}\right)^2\right) \qquad (2.7)$$

Again we have employed the anti-commutator construction to ensure Hermiticity. We have defined τ in terms of the energy unit $b^2/2m$, m

being the (average) nucleon mass.

As it turns out in the analysis of the velocity-dependent part of the Seyler-Blanchard interaction, it is of interest to introduce two additional kinetic densities κ and γ. The density κ corresponds to a velocity-squared density and is represented by the operator

$$\hat{\kappa}_i(\vec{r}) = \frac{\vec{p}_i}{b}\,\hat{\rho}_i(\vec{r})\,\frac{\vec{p}_i}{b} = \frac{\vec{p}_i}{b}\,\delta(\vec{r}-\vec{r}_i)\,\frac{\vec{p}_i}{b} \tag{2.8}$$

The density γ is the average of τ and κ and, as will be shown, corresponds to the proper quantization of the Seyler-Blanchard velocity term. It is represented by

$$\hat{\gamma}_i(\vec{r}) = \frac{1}{2}\left(\hat{\tau}_i(\vec{r}) + \hat{\kappa}_i(\vec{r})\right) = \frac{1}{4}\left\{\frac{\vec{p}_i}{b}\,,\left\{\frac{\vec{p}_i}{b}\,,\,\hat{\rho}_i(\vec{r})\right\}\right\} \tag{2.9}$$

The last relation involving the anti-commutators is elementary to prove.

It is obvious that in the classical limit ($\hbar \to 0$) all three kinetic densities τ, κ and γ are identical. In the quantum case ($\hbar \neq 0$) they are also equivalent in a region described by plane waves but they differ substantially in regions near a classical turning point. Thus the velocity-squared density κ is always positive while the kinetic-energy density τ turns negative in the classically forbidden region outside the surface. This has the consequence that the density γ, being the average of κ and τ, vanishes in an exponential-tail region.

It is straightforward to show that the two kinetic density operators $\hat{\kappa}$ and $\hat{\tau}$ are connected by the relation

$$\hat{\kappa}_i(\vec{r}) = \hat{\tau}_i(\vec{r}) - \frac{1}{2}\left[\frac{\vec{p}_i}{b}\,,\left[\frac{\vec{p}_i}{b}\,,\,\hat{\rho}_i(\vec{r})\right]\right] \tag{2.10}$$

Hence the densities themselves satisfy

$$\kappa(\vec{r}) = \tau(\vec{r}) + \frac{1}{2}\,\frac{\hbar^2}{b^2}\,\Delta\rho(\vec{r}) \tag{2.11}$$

where $\Delta\rho$ represents the Laplacian derivative of ρ.

2.1a Folded Functions

In the model under study, the potential functions are (as we shall see) generated by folding the various densities with the spatial part g of the two-body interaction. It is therefore helpful to introduce a simple notation to represent the corresponding folded functions and we shall use the corresponding capital curled letter. Thus the functions $\mathcal{R}, \vec{\mathcal{P}}, \mathcal{T}, \mathcal{K}$ and $\mathcal{G}$ are obtained from the densities ρ, $\vec{\pi}$, τ, κ and γ by folding with g. For example,

$$\mathcal{R}(\vec{r}) = \int g\left(\frac{|\vec{r} - \vec{r}'|}{a}\right)\rho(\vec{r}')\, d^3\vec{r}' \tag{2.12}$$

The differentiation operation commutes with the folding procedure, hence the relation (2.11) also holds for the folded functions,

$$\mathcal{K}(\vec{r}) = \mathcal{T}(\vec{r}) + \frac{1}{2}\,\frac{\hbar^2}{b^2}\,\Delta\mathcal{R}(\vec{r}) \tag{2.13}$$

2.2 Two-Body Interactions

We turn now to the formalism pertaining to the case when two-body interactions are present within the many-particle system.

In general, a two-particle operator acting in a system of identical particles has the form[7]

$$\hat{G} = \frac{1}{2} \sum_{ij} \hat{G}(\xi_i, \xi_j) = \frac{1}{2} \sum_{ij} \hat{G}_{ij} \tag{2.14}$$

It may change the state of two particles which implies that its matrix elements may be expressed in terms of matrix elements between two-particle states.

The evaluation of a two-particle matrix element leads to a direct term and an exchange term. In the Hartree approximation the exchange terms are neglected; this is equivalent to ignoring the antisymmetrization of the product wave function.

In the present investigation we are concerned with the limit of large systems where the effect of a single particle can be neglected. We need, therefore, not pay attention to the possible exclusion of the term corresponding to $i = j$ in the sum in (2.14); the two indices may be regarded as independent. We have introduced the brief notation $\hat{G}_{ij}$ for the term $\hat{G}(\xi_i, \xi_j)$ referring to the coordinates of particle i and j. For a system of identical particles the two-particle operator is symmetric in the particle coordinates.

For a two-body interaction the basic quantum-mechanical quantity is the operator representing the two-point interaction-energy density distribution. This two-point density operator is of the form

$$\hat{w}(\vec{r}, \vec{r}') = \frac{1}{2} \sum_{ij} \hat{w}_{ij}(\vec{r}, \vec{r}') \tag{2.15}$$

where $\vec{r}$ and $\vec{r}'$ are two spatial parameters which enter in a symmetrical way.

The corresponding two-point interaction energy density w is given

as the expectation value of the operator $\hat{w}$,

$$w(\vec{r}, \vec{r}') = \langle \hat{w}(\vec{r},\vec{r}') \rangle_\Psi = \frac{1}{2} \sum_{ij} \langle \hat{w}_{ij}(\vec{r},\vec{r}') \rangle_\Psi = \frac{1}{2} \sum_{ij} w_{ij}(\vec{r},\vec{r}') \qquad (2.16)$$

Here the contribution due to the interaction between the particles i and j is given by w_{ij}.

From this two-point density the usual one-point interaction-energy density v may be obtained by performing an integration over one argument,

$$v(\vec{r}) = \int w(\vec{r},\vec{r}') d^3\vec{r}' \qquad (2.17)$$

Furthermore, the total two-body interaction energy W may be obtained from the density v by integration over all space.

This latter quantity W, the total interaction energy, is represented by the operator $\hat{W}$ obtained from the basic interaction-energy density operator $\hat{w}$ by integration over the two spatial parameters,

$$\hat{W} = \iint \hat{w}(\vec{r}, \vec{r}') d^3\vec{r}' \, d^3\vec{r} = \frac{1}{2} \sum_{ij} \hat{W}_{ij} \qquad (2.18)$$

Thus $\hat{W}$ is a sum of contributions $\hat{W}_{ij}$ given by

$$\hat{W}_{ij} = \iint \hat{w}_{ij}(\vec{r}, \vec{r}') d^3\vec{r}' \, d^3\vec{r} \qquad (2.19)$$

This operator represents the contribution to the total interaction energy originating from the particle pair (ij).

The total interaction energy W may thus alternatively be obtained as the expectation value of the operator $\hat{W}$,

$$W = \langle \hat{W} \rangle_\Psi = \frac{1}{2} \sum_{ij} \langle \hat{W}_{ij} \rangle_\Psi = \frac{1}{2} \sum_{ij} W_{ij} \qquad (2.20)$$

where W_{ij} is the contribution due to the interaction between the particle pair (ij).

So far the formalism has been completely general. We turn now to the specific case of the Hartree approximation.

In the Hartree approximation one may introduce the effective single-particle interaction-energy operator $\hat{V}_i$ governing the motion of particle i. It represents the average effect of all the other particles and is given by

$$\hat{V}_i = \sum_j \langle \hat{W}_{ij} \rangle_j = \sum_j \int \psi^*_{\nu_j}(\vec{r}_j) \hat{W}(\vec{r}_i, \vec{r}_j) \psi_{\nu_j}(\vec{r}_j) d^3\vec{r}_j \tag{2.21}$$

The last relation is included as an illustration, it pertains to the case of the interaction being independent of spin and isospin. In the summation over j, the state i under consideration should be excluded; however, as explained above, we need not pay attention to this complication for a macroscopic system.

The total effective interaction energy operator is given by $\hat{V} = \sum \hat{V}_i$ and the total interaction energy may be obtained as

$$W = \frac{1}{2} \sum_i \langle \hat{V}_i \rangle_i \tag{2.22}$$

3. QUANTIZATION OF THE SEYLER-BLANCHARD INTERACTION

After having clarified the general formal framework we are to work within, we shall now proceed to discuss how the Seyler-Blanchard two-body interaction should be represented in a quantum-mechanical framework.

The Seyler-Blanchard interaction (1.1) depends on the positions ($\vec{r}_1$ and $\vec{r}_2$) as well as on the momenta ($\vec{p}_1$ and $\vec{p}_2$) of the two interacting particles. In general we must require that the two-body interaction be independent of which inertial frame is used as reference. For the Seyler-Blanchard interaction this invariance property is ensured by the fact that only the relative separation $r_{12} = |\vec{r}_1 - \vec{r}_2|$ and the square of the relative momentum $\vec{p}_{12} = \vec{p}_1 - \vec{p}_2$ enter. One should, however, remember that p_{12} is not in general an invariant quantity; the generally invariant quantity is the relative speed. For the present case also p_{12} is invariant because all the particles have the same mass m. It is possible to extend the standard Seyler-Blanchard interaction to the more general case of unequal masses. Moreover, such a modification would have essentially no impact on the subsequent discussion nor on the resulting formulae Hence we need not further consider this possibility.

In order to ensure a consistent derivation of the interaction-energy density as well as of the effective single-particle interaction it is in a quantum treatment necessary to start from the underlying two-point interaction-energy density operator $\hat{w}$.

The Seyler-Blanchard interaction is a sum of a velocity-independent part $V_{12}^{I} = -Cg(r_{12}/a)$ and a velocity-dependent part $V_{12}^{II} = Cg(r_{12}/a)p_{12}^2/b^2$. The quantization of the first part is rather trivial, its representation in terms of a two-point density operator simply being given by[†]

[†]In this section we shall not pay attention to the requirement that $\hat{w}_{ij}$ be symmetric in i and j. This is justified because the subsequent summation automatically yields a symmetric result. The proper $\hat{w}_{ij}$ is given as the average of (3.1) and the similar expression with i and j interchanged.

$$\hat{w}^{I}_{ij}(\vec{r}', \vec{r}'') = -Cg\left(\frac{r_{ij}}{a}\right) \hat{\rho}_i(\vec{r}')\hat{\rho}_j(\vec{r}'') \qquad (3.1)$$

The quantization of the second part is not trivial and requires special attention.

The usual quantization rule for a classical interaction written in terms of coordinates and momenta is to replace the momentum $\vec{p}$ by the corresponding differentiation operator $-i\hbar\vec{\nabla}$. This is, however, only a qualitative rule and does not provide any specific prescription for how to treat the associated commutator terms. In the choice of a specific quantization prescription, one must seek guidance in the general requirements to the quantum-mechanical interaction operator.

Thus, in general, we must require a physical interaction to be represented by a Hermitean operator. This general requirement implies that the correct algebraic prescription for quantizing a first-order product is provided by the anti-commutator construction: $f(\vec{r})\vec{p} \longrightarrow \frac{1}{2}\{\vec{p}, f\} = \frac{1}{2}(\vec{p}f + f\vec{p})$. For products involving higher powers of the momentum, however, the requirement of Hermiticity is not sufficient to uniquely determine the quantum representation of that product. In such case, no general rule has been established as of yet and one must in each specific case search for additional general requirements of physical character. We shall show below how, in our case, a unique choice is ensured by the requirement that the expression for the Seyler-Blanchard energy density refer to the momentum distribution only in terms of the total density $\vec{\pi}(\vec{r})$

rather than in terms of $\vec{\pi}^+$ and $\vec{\pi}^-$ separately.

In order to illustrate how this is brought about, and further to illuminate the difference between the various possible algebraic prescriptions, we shall in some detail consider the following two alternatives

$$\text{a)} \qquad g(\vec{r})p^2 \longrightarrow \frac{1}{2}\,(p^2 g + g p^2) \tag{3.2a}$$

$$\text{b)} \qquad g(\vec{r})p^2 \longrightarrow \vec{p}\; g\; \vec{p} \tag{3.2b}$$

Both prescriptions obviously yield a Hermitean operator, but they differ by the amount $\frac{1}{2}\hbar^2\Delta g$. Let us examine them one by one.

Illustration a)

In the quantum formalism described in Section 2 the two-body interaction-energy density operator corresponding to prescription a) [i.e., (3.2a)] is given by

$$\hat{w}^{a}_{ij}(\vec{r}',\vec{r}'') \;=\; \frac{1}{2}\left\{p_{ij}^2,\; g(r_{ij})\hat{\rho}_i(\vec{r}')\hat{\rho}_j(\vec{r}'')\right\} \tag{3.3}$$

(In this principal discussion we disregard the numerical constants a, b and C.)

We wish to deduce the corresponding energy density. Hence let us first calculate the expectation value of this operator with respect to the single-particle state ψ_{ν_j}:

$$\begin{aligned}
&\langle \hat{w}^{a}_{ij}(\vec{r}',\vec{r}'')\rangle_j \\
&= \frac{1}{2}\left\{p_i^2,\; \langle g(r_{ij})\hat{\rho}_j(\vec{r}'')\rangle_j\;\hat{\rho}_i(\vec{r}')\right\} + \left\langle\frac{1}{2}\left\{p_j^2,\; g(r_{ij})\hat{\rho}_j(\vec{r}'')\right\}\right\rangle_j \hat{\rho}_i(\vec{r}') \\
&\quad - \left(\vec{p}_i\langle\vec{p}_j\; g(r_{ij})\hat{\rho}_j(\vec{r}'')\rangle_j\;\hat{\rho}_i(\vec{r}') + \langle g(r_{ij})\hat{\rho}_j(\vec{r}'')\vec{p}_j\rangle_j\;\hat{\rho}_i(\vec{r}')\vec{p}_i\right)
\end{aligned}$$

$$= \frac{1}{2}\left\{p_i^2,\ g(r_i")\rho_j(\vec{r}")\hat{\rho}_i(\vec{r}')\right\} + g(r_i")\tau_j(\vec{r}")\hat{\rho}_i(\vec{r}')$$
$$- \left(\vec{p}_i\ g(r_i")\vec{\pi}_j^+(\vec{r}")\hat{\rho}_i(\vec{r}') + g(r_i")\vec{\pi}_j^-(\vec{r}")\hat{\rho}_i(\vec{r}')\vec{p}_i\right) \qquad (3.4)$$

We have here used the convenient abbreviation $r_i" \equiv |\vec{r}_i - \vec{r}"|$. The operator $\vec{p}_i$ does not act on the ψ_{ν_j} and may be taken outside the matrix element. This produces three types of term, one with p^2 outside, one with p^2 inside, and crossterms with one $\vec{p}$ outside and one $\vec{p}$ inside. In the last expression we have, wherever possible, introduced the various densities defined in Subsection 2.1. Next, we form the expectation value with respect to ψ_{ν_i}:

$$\langle\langle w_{ij}^a(\vec{r}', \vec{r}")\rangle_j\rangle_i = w_{ij}^a(\vec{r}', \vec{r}")$$
$$= g(r)\tau_i(\vec{r}')\rho_j(\vec{r}") + g(r)\rho_i(\vec{r}')\tau_j(\vec{r}")$$
$$- \left(g(r)\vec{\pi}_i^+(\vec{r}') \cdot \vec{\pi}_j^+(\vec{r}") + g(r)\vec{\pi}_i^-(\vec{r}') \cdot \vec{\pi}_j^-(\vec{r}")\right) \qquad (3.5)$$

where we have introduced $r = |\vec{r}' - \vec{r}"|$. Finally, summation over all pairs results in the total two-point interaction-energy density

$$w^a(\vec{r}', \vec{r}") = \frac{1}{2}\sum_{ij} w_{ij}^a(\vec{r}', \vec{r}") \qquad (3.6)$$
$$= \frac{1}{2}\,g(r)\left(\tau(\vec{r}')\rho(\vec{r}") + \rho(\vec{r}')\tau(\vec{r}") - \left(\vec{\pi}^+(\vec{r}') \cdot \vec{\pi}^+(\vec{r}") + \vec{\pi}^-(\vec{r}') \cdot \vec{\pi}^-(\vec{r}")\right)\right)$$

At this point, we wish to draw the attention to the fact that in this expression the momentum density is represented through its two constituents $\vec{\pi}^+$ and $\vec{\pi}^-$ separately rather than by the sum of them.

The dependence on the momentum density is generated by the cross terms. We notice that the contributions from the p^2 terms are given in

terms of the kinetic-energy density τ. This is because the construction a is characteristic of the kinetic energy, cfr. eq. (2.7).

Illustration b)

Now let us perform a similar analysis of the alternative prescription b. In this case the basic density operator is given by

$$w^{b}_{ij}(\vec{r}', \vec{r}'') = \vec{p}_{ij}\, g(r_{ij})\hat{\rho}_i(\vec{r}')\hat{\rho}_j(\vec{r}'')\vec{p}_{ij} \tag{3.7}$$

The derivation of the energy density is rather similar to the previous one but we shall exhibit the various steps in order that comparison can be made and the occurring differences understood. Thus, take first the expectation value with respect to ψ_{ν_j},

$$\begin{aligned}
&\langle w^{b}_{ij}(\vec{r}', \vec{r}'')\rangle_j \\
&= \vec{p}_i\langle g(r_{ij})\hat{\rho}_j(\vec{r}'')\rangle_j\, \hat{\rho}_i(\vec{r}')\vec{p}_i + \langle \vec{p}_j\, g(r_{ij})\hat{\rho}_j(\vec{r}'')\vec{p}_j\rangle_j\, \hat{\rho}_i(\vec{r}') \\
&- \left(\vec{p}_i\langle g(r_{ij})\hat{\rho}_j(\vec{r}'')\vec{p}_j\rangle_j\, \hat{\rho}_i(\vec{r}') + \langle \vec{p}_j\, g(r_{ij})\hat{\rho}_j(\vec{r}'')\rangle_j\, \hat{\rho}_i(\vec{r}')\vec{p}_i\right) \\
&= \vec{p}_i\, g(r_i'')\rho_j(\vec{r}'')\hat{\rho}_i(\vec{r}')\vec{p}_i + g(r_i'')\kappa(\vec{r}'')\hat{\rho}_i(\vec{r}') \\
&- \left(\vec{p}_i\, g(r_i'')\vec{\pi}^{-}_j(\vec{r}'')\hat{\rho}_i(\vec{r}') + g(r_i'')\vec{\pi}^{+}_j(\vec{r}'')\hat{\rho}_i(\vec{r}')\vec{p}_i\right)
\end{aligned} \tag{3.8}$$

and then with respect to ψ_{ν_i},

$$\begin{aligned}
&\langle\langle w^{b}_{ij}(\vec{r}', \vec{r}'')\rangle_j\rangle_i = w^{b}_{ij}(\vec{r}', \vec{r}') \\
&= g(r)\kappa_i(\vec{r}')\rho_j(\vec{r}'') + g(r)\rho_i(\vec{r}')\kappa_j(\vec{r}'') \\
&- \left(g(r)\vec{\pi}^{+}_i(\vec{r}') \cdot \vec{\pi}^{-}_j(\vec{r}'') + g(r)\vec{\pi}^{-}_i(\vec{r}') \cdot \vec{\pi}^{+}_j(\vec{r}'')\right)
\end{aligned} \tag{3.9}$$

Finally, sum over all pairs,

$$w^b(\vec{r}', \vec{r}'') = \frac{1}{2} \sum_{ij} w^b_{ij}(\vec{r}', \vec{r}'') \tag{3.10}$$

$$= \frac{1}{2} g(r) \Big(\kappa(\vec{r}')\rho(\vec{r}'') + \rho(\vec{r}')\kappa(\vec{r}'') - \big(\vec{\pi}^+(\vec{r}') \cdot \vec{\pi}^-(\vec{r}'') + \vec{\pi}^-(\vec{r}') \cdot \vec{\pi}^+(\vec{r}'') \big) \Big)$$

We notice that in this case the p^2 contributions are given in terms of the density κ because this density is defined by a construction analogous to prescription b), cfr. eq. (2.8). Of course, by virtue of the connection formula (2.11), the above expression may be rewritten in terms of τ; this would add a term containing $\Delta\rho$.

Furthermore, we observe that alternative b) is no better than alternative a) in producing an acceptable dependence on the momentum density.

How undesirable this appearance of the partial momentum densities is may be illustrated by the simple case of a static system described by standing waves. In such a system there is no net flow and there should be no momentum contribution to the energy density. Nevertheless, the first alternative yields a contribution $\delta w^a = \frac{1}{4}\hbar^2 g(r) \vec{\nabla}\rho(\vec{r}') \cdot \vec{\nabla}\rho(\vec{r}'')$ while choice b) contributes just the negative of that amount. In regions of constant density there is no contribution but where the density varies rapidly, as for example in the surface region, there is a considerable effect.

From the above analysis it is now clear that the additional requirement, that the resulting energy density only involve the total momentum distribution and not its (unphysical) constituents separately, leads to a unique prescription for the quantization of the velocity-dependent part of the Seyler-Blanchard interaction. And moreover, as

is readily seen, this unique algebraic prescription is just the average of the two illustrative alternatives considered in detail above, $w = \frac{1}{2}(w^a + w^b)$.

We thus conclude that the proper quantum representation of the velocity-dependent part of the Seyler-Blanchard interaction is given in terms of the following density operator

$$\hat{w}^{II}_{ij}(\vec{r}', \vec{r}'') = C\frac{1}{4}\left\{\frac{\vec{p}_{ij}}{b}, \left\{\frac{\vec{p}_{ij}}{b}, g\left(\frac{r_{ij}}{a}\right)\hat{\rho}_i(\vec{r}')\hat{\rho}_j(\vec{r}'')\right\}\right\} \tag{3.11}$$

It is satisfactory to see that this specific algebraic prescription for quantizing the second order product gp^2 simply corresponds to the successive application of the anti-commutator construction $gp^2 \longrightarrow \frac{1}{4}\{\vec{p}, \{\vec{p}, g\}\}$. This prescription thus constitutes an appealing generalization of the similar rule pertaining to a first order product.

From the analysis performed above it is easy to verify that the resulting expression for the Seyler-Blanchard interaction-energy density itself is given by

$$\begin{aligned} w(\vec{r}', \vec{r}'') = & -\frac{1}{2}Cg\left(\frac{r}{a}\right)\Big(\rho(\vec{r}')\rho(\vec{r}'') - \gamma(\vec{r}')\rho(\vec{r}'') \\ & - \rho(\vec{r}')\gamma(\vec{r}'') + 2\vec{\pi}(\vec{r}') \cdot \vec{\pi}(\vec{r}'')\Big) \end{aligned} \tag{3.12}$$

4. GENERAL RESULTS

After having thus settled the problem of quantizing the velocity dependent interaction we now proceed to the general formulation of the model in the Hartree approximation.

4.1. Multi-Component Systems

In general one may deal with a system composed of several different components. In the nuclear case we have two components, neutrons and protons, but as it poses no additional difficulties we shall formulate the model for the general case of any number of components. The various components are denoted by α, β, ... We shall keep the assumption that all particles have equal masses. The more general case where the masses differ for different components may be treated in an analogous way but requires certain refinements as well concerning the two-body interaction as concerning the various densities in terms of which the physical properties of the system are described. This assumption has no implications for the subsequent applications to nuclear matter. Thus, all the particles have equal masses but the interaction strength between two particles depends on which two components the particles belong to. This may be expressed as follows,

$$C(i\varepsilon\alpha,\ j\varepsilon\beta) \ = \ C_{\alpha\beta} \tag{4.1}$$

Thus the interaction-strength constants form a symmetric matrix $\mathbf{C} = \{C_{\alpha\beta}\}$. Furthermore, the various density-distributions introduced in Subsection 2.1 for a one-component system have now the structure of one-dimensional matrices (for example: $\rho(\vec{r}) = \{\rho_\alpha(\vec{r})\}$) with one element pertaining to each of the components. The total density of the combined system is then the sum of contributions from each component ($\rho_{tot}(\vec{r}) = \sum_\alpha \rho_\alpha(\vec{r})$).

Fortunately, the complication of having more than one component

in the system does not influence the general formulae in the model, provided that we interpret products involving the interaction strength in terms of matrix multiplications. To remind ourselves of the possible multi-component structure of such products we shall write the interaction strength as $\mathbf{C}$ rather than C. Thus, for example,

$$\rho(\vec{r})\ \mathbf{C}\mathcal{R}(\vec{r}) = \sum_{\alpha\beta} \rho_\alpha(\vec{r})\ C_{\alpha\beta}\ \mathcal{R}_\beta(\vec{r}) \tag{4.2}$$

With this interpretation all the formulae derived in the following have general validity.

4.2. General Expressions

As mentioned in Section 3, a consistent quantum treatment requires the knowledge of the two-body interaction-energy *density* operator $\hat{w}$ from which the energy density as well as the effective single-particle interaction operator derive. It emerges from the discussion in Section 3 that for the Seyler-Blanchard interaction this operator is properly given by

$$\begin{aligned}\hat{w}(\vec{r}', \vec{r}'') &= \frac{1}{2}\sum_{ij} \hat{w}_{ij}(\vec{r}', \vec{r}'') \\ &= \frac{1}{2}\sum_{ij} C_{\alpha\beta}\left(g\left(\frac{r_{ij}}{a}\right)\hat{\rho}_i(\vec{r}')\hat{\rho}_j(\vec{r}'') - \frac{1}{4}\left\{\frac{\vec{p}_{ij}}{b}, \left\{\frac{\vec{p}_{ij}}{b}, g\left(\frac{r_{ij}}{a}\right)\hat{\rho}_i(\vec{r}')\hat{\rho}_j(\vec{r}'')\right\}\right\}\right)\end{aligned} \tag{4.3}$$

where $i\varepsilon\alpha$ and $j\varepsilon\beta$. This operator represents the two-point interaction-energy density generated by the Seyler-Blanchard interaction in the given system. The corresponding classical quantity is given by the same expression, with the interpretation that $\vec{p}_{ij}$ is just the classical relative momentum.

The two-point interaction-energy density w is obtained from the above operator by forming the expectation value with respect to system considered. This leads to

$$w(\vec{r}', \vec{r}'') \tag{4.4}$$
$$= -\frac{1}{2}g\left(\frac{r}{a}\right)\left(\rho(\vec{r}')\mathbb{C}\rho(\vec{r}'') - \gamma(\vec{r}')\mathbb{C}\rho(\vec{r}'') - \rho(\vec{r}')\mathbb{C}\gamma(\vec{r}'') + 2\vec{\pi}(\vec{r}')\mathbb{C}\vec{\pi}(\vec{r}'')\right)$$

where $r = |\vec{r}' - \vec{r}''|$. This expression is valid as well in classical as in quantum mechanics. Moreover, its validity extends to the general case of a non-static system, for which $\vec{\pi} \neq \vec{0}$.

From the two-point density the one-point interaction-energy density v may be derived by integrating over one of the spatial parameters.

$$2v(\vec{r}) = -\rho(\vec{r})\mathbb{C}\mathcal{R}(\vec{r}) + \gamma(\vec{r})\mathbb{C}\mathcal{R}(\vec{r}) + \rho(\vec{r})\mathbb{C}\mathcal{G}(\vec{r}) - 2\pi(\vec{r})\mathbb{C}\vec{\mathcal{P}}(\vec{r}) \tag{4.5}$$

We have here made use of the notation introduced in Subsection 2.1a that the curly letters denote the folded functions. Again, of course, this expression has general validity.

The two-body operator $\hat{W}$ representing the total interaction energy is obtained from the two-point density operator $\hat{w}$ by integration over both spatial parameters. Hence it is given by

$$\hat{W} = -\frac{1}{2}\sum_{ij} C_{\alpha\beta}\left(g\left(\frac{r_{ij}}{a}\right) - \left\{\frac{\vec{p}_{ij}}{b}, \left\{\frac{\vec{p}_{ij}}{b}, g\left(\frac{r_{ij}}{a}\right)\right\}\right\}\right) \tag{4.6}$$

where $i\varepsilon\alpha$ and $j\varepsilon\beta$. As was the case for $\hat{w}$, the classical interaction corresponding to $\hat{W}$ is given by the same expression, with the classical interpretation of the momenta.

Up to now, our results have been completely general. Let us now concentrate on the Hartree approximation. As noted in Section 2, the particular simplicity emerging in the Hartree approximation is the existence of an effective interaction governing the motion of the individual particles. This effective single-particle operator $\hat{V}$ is given by

$$\hat{V}_i(\vec{r}_i) = \iint \sum_j \langle \hat{w}_{ij}(\vec{r}', \vec{r}'') \rangle_j \, d^3\vec{r}'' \, d^3\vec{r}' =$$

$$- \mathfrak{C}\mathcal{R}(\vec{r}_i) + \frac{1}{4}\left\{\frac{\vec{p}_i}{b}, \left\{\frac{\vec{p}_i}{b}, \mathfrak{C}\mathcal{R}(\vec{r}_i)\right\}\right\} + \mathfrak{C}\mathcal{G}(\vec{r}_i) - \left\{\frac{\vec{p}_i}{b}, \mathfrak{C}\vec{\mathcal{P}}(\vec{r}_i)\right\} \qquad (4.7)$$

At this point it is worthwhile noticing that since the density γ has the form:

$$\gamma_i = \langle \hat{\gamma}_i \rangle_i = \frac{1}{4}\left(\psi^*_{\nu_i}\left(\frac{p_i^2}{b^2}\psi_{\nu_i}\right) + 2\left(\frac{\vec{p}_i}{b}\psi_{\nu_i}\right)^*\left(\frac{\vec{p}_i}{b}\psi_{\nu_i}\right) + \left(\frac{p_i^2}{b^2}\psi_{\nu_i}\right)^*\psi_{\nu_i}\right) \qquad (4.8)$$

it is *not* possible to generate the interaction-energy density v from the effective one-particle operator $\hat{V}$. Thus, for example

$$2v_i \neq \frac{1}{2}\left(\psi_{\nu_i}{}^*(\hat{V}_i\psi_{\nu_i}) + (\hat{V}_i\psi_{\nu_i})^*\psi_{\nu_i}\right) \qquad (4.9)$$

The difference integrates up to zero over all space but locally it may be substantial, particularly in the surface region. This fact indicates the importance of having a consistent formalism including the underlying density operators.

The effective single-particle operator $\hat{V}_i$ depends on which component α the particle belongs to. The first and third terms contribute to the static potential felt by the individual particles in component α. The second term contains the velocity squared and hence adds to the free kinetic energy of the particle by way of renormalizing the inertial mass for the particle; this renormalized mass depends on the particle position $\vec{r}$. The last term has a linear velocity dependence and produces an additional force in case there is internal gross flow in the system.

4.3 Effective Single-Particle Hamiltonian

We have now carried through the derivation of the various general expressions pertaining to the Seyler-Blanchard two-body interaction. The motion of the individual particles in the system is governed by the corresponding effective single-particle Hamiltonian H_i, which is the free kinetic-energy operator $p_i^2/2m$ plus the effective interaction-energy operator $\hat{V}_i$. The effective Hamiltonian depends on which component α the particle i belongs to.

The algebraic form of the momentum-dependence in the effective interaction operator (4.7) reflects the specific construction used in the quantization of the velocity-dependent term in the Seyler-Blanchard interaction. For practical applications it is more convenient to rewrite the Hamiltonian in a simpler form. This is possible by virtue of the relation (2.13) connecting the various kinetic constructions to each other. Thus it is elementary to show that the effective single-particle Hamiltonian may be cast into the form

$$H_\alpha = \vec{P}_\alpha \frac{1}{2B_\alpha} \vec{P}_\alpha + U_\alpha \tag{4.10}$$

This form of the kinetic term leads to a Schrödinger equation which is easy to treat numerically (cfr. Appendix A). We have introduced the following three position-dependent quantities pertaining to particles from component α.

1) Effective mass $B_\alpha(\vec{r})$

$$\frac{1}{2B_\alpha(\vec{r})} = \frac{1}{2m}\left(1 + \frac{2m}{b^2} C\mathcal{R}(\vec{r})\right) \tag{4.11}$$

The existence of an effective mass function is a direct consequence of the velocity-squared dependence of the two-body interaction. The effective mass is equal to the free mass outside the system (where $\mathcal{R} = 0$) while it is smaller within the field of the system.

2) Effective momentum $\vec{P}_\alpha(\vec{r})$

$$\vec{P}_\alpha(\vec{r}) = \vec{p} - B_\alpha(\vec{r})\vec{\mathcal{U}}_\alpha(\vec{r}) \tag{4.12}$$

where $\vec{\mathcal{U}}_\alpha(\vec{r}) = \frac{b}{m}\frac{2m}{b^2} C\vec{\mathcal{P}}_\alpha(\vec{r})$. The introduction of an effective momentum permits us to write the Hamiltonian in the simple form (4.10). The quantity $\vec{\mathcal{U}}$ plays the role of an effective overall velocity distribution and only contributes if the system is not everywhere at rest.

3) Effective static potential $U_\alpha(\vec{r})$

$$U_\alpha(\vec{r}) = -C\mathcal{R}(\vec{r}) + C\mathcal{T}(\vec{r}) - \frac{1}{2} B_\alpha(\vec{r}) \mathcal{U}_\alpha(\vec{r})^2 \tag{4.13}$$

The first term is the contribution from the momentum-independent part

of the two-body interaction while the second term originates from the momentum-dependent term.

The presence of the terms containing $\vec{\mathcal{U}}$ in $\vec{P}$ and U ensures that the interaction energy is unaffected by an overall translational velocity of the system. Furthermore, one should notice that the potential U is defined in terms of $\mathcal{T}$ rather than $\mathcal{G}$; this is a consequence of the rearrangement of the kinetic term in the Hamiltonian (4.10). Therefore, when written in the form (4.10), the effective Hamiltonian may be established from knowledge of the primary densities ρ, $\vec{\pi}$ and τ alone; it is not necessary to also know γ.

4.4 Self-Consistent Solution

The definition of the various density distributions in terms of the single-particle wave functions ψ_{ν_i}, together with the effective single-particle Schrödinger equation generating these wave functions, provide us with a simple iteration procedure for obtaining the self-consistent solution to the many-body problem.

Thus, starting out with some approximate density distributions ρ, $\vec{\pi}$ and τ, the potential functions $\mathcal{R}$, $\vec{\mathcal{P}}$ and $\mathcal{T}$ entering in the effective Hamiltonian are generated by folding with the spatial function g. Having established in this way the effective single-particle Hamiltonian H_α, we subsequently solve the corresponding Schrödinger equation

$$H_\alpha \psi_{\nu_i} = E_{\nu_i} \psi_{\nu_i} \tag{4.14}$$

for every particle i. This yields a set of wave functions from which

modified density distributions ρ', $\vec{\pi}'$ and τ' may be obtained. The procedure is repeated until sufficient self-consistency has been reached.

This iteration scheme is conceptually very simple, and our experience from actual applications indicates that the scheme will exhibit a rather fast convergence for all reasonable initial conditions.

In the asymptotic bulk region of the system, where the potential is constant and the surface far away, this solution yields results identical to those of the Thomas-Fermi approximation, but, as we shall see, interference effects originating from the surface may persist deep into the system in the Hartree approximation.

4.4a Thomas-Fermi Approximation

It is of interest at this point to discuss the connection of the Thomas-Fermi approximation employed in refs. 1, 3 and 4 to the general quantum-mechanical framework derived above.

In the Thomas-Fermi approximation, the system is locally treated as the equivalent infinite homogeneous system. Since an infinite homogeneous system may be described by plane waves, the Thomas-Fermi approximation is often formulated as that of treating the single-particle wave function ψ_ν as a plane wave, with wave number and normalization factor determined from classical considerations (this implies that particles are not permitted to penetrate into a classically forbidden region).

With this approximation the summation over states becomes trivial. Remembering that for a plane wave the momentum operator acts simply as a multiplication operator, we thus arrive at the following expressions for the density ρ and the kinetic-energy density τ (assuming the system

to be at rest).

$$\rho(\vec{r}) = \frac{t}{h^3}\int^{P_F} d^3\vec{p} = \frac{4\pi}{3}\, t\, \frac{P_F^3}{h^3}$$

$$\tau(\vec{r}) = \frac{t}{h^3}\int^{P_F} \frac{p^2}{b^2}\, d^3\vec{p} = \frac{3}{5}\, \frac{P_F^2}{b^2}\, \rho \qquad (4.15)$$

where $t = 4$ is the spin-isospin degeneracy. The local Fermi momentum $P_F(\vec{r})$ is determined from the condition of a constant Fermi energy E_F,

$$E_F = P_F(\vec{r})^2 / 2B(\vec{r}) + U(\vec{r}) \qquad (4.16)$$

One might notice that for the Thomas-Fermi system the energy density e may be written as

$$e(\vec{r}) = \frac{1}{2}\left(\varepsilon(\vec{r}) + \tau(\vec{r})\right)\frac{b^2}{2m} \qquad (4.17)$$

where the "eigenvalue" density ε is given by

$$\varepsilon(\vec{r}) = \frac{m}{B(\vec{r})}\, \tau(\vec{r}) + \frac{2m}{b^2}\, U(\vec{r})\, \rho(\vec{r}) \qquad (4.18)$$

It should be realized that one must exercise care when incorporating the Thomas-Fermi approximation into a quantum-mechanical scheme. It is a characteristic feature of the approximation that when calculating the action of the momentum operator on the single-particle wave function the variation of the normalization factor is neglected. This implies that the Thomas-Fermi approximation cannot be formulated in terms of specific approximate wave functions which are subsequently treated consistently within the quantal framework. Thus the Thomas-Fermi approximation is

conceptually closer to a classical treatment than, for example, the WKB approximation, despite the fact that they yield similar density distributions (in the classically allowed region).

5. SEMI-INFINITE SYMMETRIC NUCLEAR MATTER

We have now completed the general development of the model in the Hartree approximation. We shall then proceed to study the effect of the quantization on the surface structure of symmetric nuclear matter. We shall report elsewhere on other applications.

Thus, we shall here consider a semi-infinite system with identical neutron and proton distributions. In Appendix A we describe the corresponding specialization of the formalism and, furthermore, outline the various numerical methods used for the actual computation.

Our primary aim in this section is to study the results of the quantization relative to the Thomas-Fermi approximation. We therefore choose the values of the physical input parameters determined in ref. 2. They are

$$\begin{aligned} a &= 0.62567 \text{ fm} \quad \text{(Yukawa range)} \\ b &= 372.48 \text{ MeV} \quad \text{(Saturation momentum)} \\ C &= 328.61 \text{ MeV} \quad \text{(Interaction strength)} \end{aligned} \tag{5.1}$$

These values were determined from the extracted experimental values for the nuclear-matter binding energy, the nuclear-matter density and the nuclear surface energy as they are given in terms of the volume-energy coefficient $a_v = 15.667$ MeV, the radius constant $r_o = 1.2049$ fm, and the surface-energy coefficient $a_s = 18.560$ MeV. The (average) nucleon mass

is $m = 938.903\ \mathrm{MeV}/c^2$. It should be added that for the case of identical neutron and proton distributions the problem reduces effectively to that of a one-component system and the corresponding interaction strength is simply the average value $C = \frac{1}{2}(C_\ell + C_{\ell\ell})$, cfr. Appendix A and ref. 2.

5.1. Density Profiles

For the parameter values specified above we have calculated the self-consistent solution to the derived Hartree equations. In fig. 1 we display the resulting matter density distribution $\rho(x)$. For comparison we also show the corresponding density distribution as obtained in the Thomas-Fermi approximation. The two densities are plotted such that their surface locations x_s coincide. The Hartree density exhibits two new features relative to the Thomas-Fermi density. One is the tail outside the system due to the finite depth of the nuclear potential. The other feature is the density ripples due to the phase correlations imposed by the presence of the surface.

We observe that the Thomas-Fermi density represents the average trend of the Hartree density quite well, being most markedly off in the tail region. The surface diffuseness, measured in terms of the 10 - 90% distance, increases by around 11% from 3.17a to 3.51a. This increase is almost entirely due to the density tail which moves the 10% point outwards by 0.46a. The 90% point is almost unaffected by the quantization because it happens to be located right between two oscillations.

The density ripples deserve some special attention and we may illuminate the situation by comparing with the extreme case of an infinitely high potential wall. In this case the density ripples are very pronounced,

being given by the well-known expression

$$\rho(x)/\rho_o = 1 + \frac{3}{\bar{X}^2}\cos\bar{X} - \frac{3}{\bar{X}^3}\sin\bar{X} \ , \quad \bar{X} = 2P_F\, x/\hbar \qquad (5.2)$$

where ρ_o is the asymptotic bulk density. This fictional density is indicated on the figure by the dashed curve; it is drawn to be in phase with the calculated ripples in the bulk region. We observe that the amplitudes of the calculated ripples are considerably smaller than those corresponding to a sharp surface. This is due to the diffuse surface which disturbs to some extent the perfect phase correlations of the wave functions at the surface and thereby inhibits the undulations.

However, as one goes away from the surface region deeper into the system the effect of the surface profile is felt to a decreasing extent and the wiggles become more and more similar to those pertaining to a sharp wall.† This phenomenon is illustrated in fig. 2 where we have plotted the amplitude versus the depth from the surface. Thus the asymptotic behavior does not depend on the detailed profile of the surface but follows in general the infinite-wall expression (5.2).

This fact has some impact on the possibility of describing the density profile in terms of surface moments along the lines suggested by Süssmann for finite nuclei.[9] Süssmann has advocated the idea that

---

†In their study of nuclear density oscillations, Thorpe and Thouless[8] show that asymptotically the density oscillations pertaining to a diffuse semi-infinite potential are essentially only modified by an overall phase shift relative to the infinite-wall oscillations. Furthermore they state that for the diffuse potential the first density hump may drop from its infinite-wall value of 8.6% to as little as 1.6% above the Thomas-Fermi density. In our case the first hump exceeds the Thomas-Fermi density by approximately 2.5%.

the nuclear density profile be described in terms of surface moments of the density distributions, the surface diffuseness being given in terms of the second moment, the surface skewness (flare) in terms of the third moment, and so on. Any two distributions may then be compared by comparing their respective surface moments. However, as we have seen above, asymptotically the density amplitudes are inversely proportional to the square of the depth. Consequently all higher moments, from the second and up, are not mathematically well defined. In fact, they all exhibit an oscillatory behavior as function of the lower limit of the integral (the cut-off depth $x_<$), the corresponding amplitude being constant for the second moment, increasing linearly for the third moment, and so on. Hence it is not possible to directly extract the surface-moment information about a semi-infinite quantum density distribution. For real nuclei, of course, the problem does not occur because of the finite size. But it is of general interest to study semi-infinite systems. And since this type of density ripple is a quite general feature in a Hartree description of such systems, it would be desirable to generalize the concept of surface moments to cover this case as well. Such a generalization could conceivably be brought about by defining some appropriate averaging procedure by which the convergence would be ensured. In doing so one might benefit from the general knowledge of the behavior of the ripples in the asymptotic limit.

A very rough attempt along such lines has been done for the surface width by simple graphical averaging of the integral as function of its lower limit. Such a procedure seems relatively reliable for the width and the result may be compared with the Thomas-Fermi value (cfr. Table 1).

But for the higher moments a more rigorous mathematical prescription is required.

We see that the second-moment width b increases from 1.39a to approximately 1.47a which is only 6%. The main part of this increase is due to the density tail while the phase of the wiggles is such that there is a relatively small contribution to the width integral from the interior region.

In fig. 3 we have made a similar plot of the kinetic-energy densities obtained in the Hartree and Thomas-Fermi approximations. We observe here in particular how the kinetic-energy density is negative in the outer surface region. But apart from this region it follows rather closely the oscillations of the matter distribution plotted in fig. 1.

In the quantum expression (4.5) for the Seyler-Blanchard interaction-energy density the velocity dependence is represented through the kinetic density γ (rather than the kinetic-energy density τ). The behavior of γ is seen in fig. 4 where we have plotted τ, γ and the "velocity-squared" density κ. It should be noted that the oscillations of the two densities τ and κ are just opposite.† Consequently γ, which is the average of τ and κ, is a rather smooth density in the bulk. Furthermore we observe that in the tail region γ remains positive but tends rather rapidly to zero.‡

---

†Current studies performed by Gräf[10] with the generalized Thomas-Fermi approximation introduced by Swiatecki[11] indicate that this tendency of cancellation between τ and κ is a quite general feature.

‡This is also in accordance with the general results obtained by Gräf.[10]

We recall the fact mentioned before that in a forbidden region under a constant potential, γ would be strictly zero.

5.2 Surface Energy

For the self-consistent Hartree solution we have calculated the surface-energy density distribution $a_s(x)$. The surface energy represents the binding-energy deficit due to the presence of a surface for the system. Hence $a_s(x)$ is given by

$$a_s(x) = e(x) - \frac{e_o}{\rho_o}\rho(x) \tag{5.12}$$

where $e(x)$ is the total energy density and $\rho(x)$ the matter density. The subscripts o refer as usual to the bulk values. The surface-energy coefficient a_s is the integral of this density, multiplied by the 'nucleon' surface area,

$$a_s = 4\pi r_o^2 \int_{-\infty}^{\infty} a_s(x)\, dx \tag{5.13}$$

In fig. 5 we show the calculated surface-energy density together with the one pertaining to the Thomas-Fermi system. Figure 6 shows the decomposition of these densities into their kinetic and interaction parts. For the Hartree system those latter partial densities exhibit oscillations in the deeper part of the system. They are opposite to each other so that the combined density $a_s(x)$ has considerably smaller oscillations. The Thomas-Fermi densities all go to zero at end-point $x_o \simeq 1.90a$ while the Hartree densities extend out in the tail region. We notice that in this region the two parts tend to cancel each other

resulting in a rather negligible, slightly negative, value of the total surface-energy density.

The kinetic-energy contribution to the surface-energy density is negative (apart from the small bulk oscillations). Its behavior in the tail region reflects the fact that it is very advantageous for a particle to be in this region as it has here very small or even negative kinetic energy. Further inside the system the Hartree contribution is less negative than the Thomas-Fermi contribution. This is due to the quantum localization effect which prohibits low-momentum particles from getting as close to a potential wall as high-momentum particles. This exclusion of the low-momentum particles from the potential surface results in a relative excess of high-momentum particles and a corresponding higher kinetic energy in that region. In the Thomas-Fermi approximation, with its phase averaging, this effect is not taken into account. In the extreme case of a sharp wall, the kinetic-energy contribution to the surface energy would be positive; the fact that it remains negative in the actual case is due to the diffuseness of the surface.

The interaction-energy contribution to the surface-energy density follows more closely the Thomas-Fermi curve, with some wiggles reflecting the matter-density oscillations relative to the Thomas-Fermi density. For example, the fact that $a_x^{int}(x)$ is smaller than the Thomas-Fermi curve on the inside slope (around -3a) is a consequence of the first density hump which brings the density closer to the ideal bulk value and consequently lowers the energy deficit. In the tail region there is an appreciable contribution because the particles here are not very

well bound. As we noticed, it so happens that this contribution to a large extent cancels the kinetic-energy gain in the tail.

The curve for the total surface-energy density then follows rather well the Thomas-Fermi curve. The largest deviation occurs near the peak and from the discussion above it follows that this increase should be mainly ascribed to the lack of low-momentum particles near a quantum surface.

The integrated quantities corresponding to the various densities discussed above are listed in Table 1. For the surface-energy coefficient a_s we find a 10% increase from the Thomas-Fermi value of 18.56 MeV to 20.51 MeV. In an earlier study by Köhler[12] of nuclear many-body calculations it is stated that the surface-energy coefficient would increase by 3.3 ± 1 MeV. This trend is confirmed by the present more accurate finding that the increase is 1.95 ± 0.01 MeV; because of the large error quoted by Köhler we do not attempt a detailed comparison.

5.3 Potentials

The single-particle motion in the system is governed by the effective mass function B and the effective static potential U. We have displayed these two functions in fig. 7 together with their Thomas-Fermi analogues. We see that the main difference is a somewhat larger 10 - 90% diffuseness for the Hartree curves. This increase is to a large part due to the density tail which causes the potential functions to extend further out than in the Thomas-Fermi case.

Let us terminate this presentation of the numerical results by returning to the problem of the commutator terms discussed in detail in Section 3. We saw then that the various alternative suggestions for the algebraic form of the momentum dependence lead to different effective static potentials. In particular we have:

$$U^a + \delta U = U = U^b - \delta U \tag{5.14}$$

where U^a and U^b are the potentials pertaining to the two illustrative choices a and b. The potential δU arises from the commutator terms when the effective Hamiltonians are rewritten in the same form. It is given by

$$\delta U = -\frac{1}{2}\left[\frac{\vec{p}}{b}, \left[\frac{\vec{p}}{b}, \mathcal{C}\mathcal{R}\right]\right] = \frac{1}{2}\frac{\hbar^2}{b^2}\Delta\mathcal{C}\mathcal{R} \tag{5.15}$$

In fig. 8 this potential is shown for the actual case considered above. The corresponding potentials U^a and U^b are also displayed. It is clear that the effect of adding δU is an increase in the surface diffuseness, as it turns out, of around 0.5a. The two potentials U^a and U^b differ in diffuseness by more than one Yukawa range. This indicates the importance of being cautious when quantizing the momentum-dependent interaction.

6. SUMMARY AND DISCUSSION

The principal purpose of the investigation reported here was to formulate in the Hartree approximation the macroscopic nuclear model based on the Seyler-Blanchard interaction. Let us now summarize.

First we have described a general formalism with which that kind of problem may be treated. It is particularly important that the formalism employed contains in a consistent way the concept of densities; in our formalism this is ensured by taking as the basic quantities the quantum-mechanical *density operators* from which the density distributions are generated as expectation values. The formalism developed will also be useful when further developments of the model are considered.

With the aid of this formalism we have studied in detail how the velocity-dependent Seyler-Blanchard interaction may be quantized. It was shown that the additional criterion that the ensuing energy density depend only on physical (i.e., Hermitean) quantities leads to a unique quantum representation of the interaction. It is important at this point to distinguish between the various types of kinetic density.

Having settled this problem we proceeded to derive the general formulae for the interaction-energy density and the effective single-particle interaction-energy operator. This operator may be combined with the free kinetic-energy operator to form the effective single-particle Hamiltonian governing the motion of the individual particles. The Hamiltonian contains a static potential and an effective mass, both position-dependent; in addition, the momentum is modified locally for systems with internal gross flow. These quantities, entering into the Schrödinger equation, are obtained by folding the various density distributions with the two-body Yukawa interaction. This establishes a conceptually simple iterative scheme for obtaining the self-consistent solution to the many-body problem.

The model developed was applied to semi-infinite symmetric nuclear matter. The geometrical properties of the quantum density profiles were studied and it was demonstrated that the conventional description in terms of surface moments cannot directly be applied because of the persistence deep into the system of the density ripples caused by the surface.

Next, we studied the nuclear surface energy. Its distribution through the surface region was compared with the Thomas-Fermi results and the origin of the deviations identified. The 10 - 90% surface thickness as well as the surface-energy coefficient were found to increase by around 11%, the thickness because of the extended density tail and the surface energy mostly because of the relative lack of low-momentum particles near the surface.

Finally, we presented the effective mass function and the effective static potential governing the motion of the individual particles. They are both more diffuse than in the Thomas-Fermi approximation; this is mainly a consequence of the extended density tail of the matter distribution. It was furthermore demonstrated that the commutator terms in the quantized model have an appreciable influence on the surface diffuseness of the single-particle potential. This indicates the importance of treating the quantum algebra consistently.

Our study of the semi-infinite nuclear system may be concluded by the following remarks. For the various density distributions, the Thomas-Fermi approximation yields a good average representation of the Hartree results. This supports the application of the Thomas-Fermi approximation for studies of macroscopic nuclear properties. In this

connection we recall the criterion derived in ref. 2 that the Thomas-Fermi approximation yields the correct density to within 10% provided $|\vec{\nabla}\rho|/\rho^{4/3} \lesssim 10$. In the nuclear case this relation holds good through the surface region out to a point where the density has dropped to one-sixth of its central value.[2] Our results, displayed in figs. 1 and 3, are seen to confirm this criterion which was obtained on the basis of a study of linear potentials.[11] Furthermore, we can state that the Thomas-Fermi approximation underestimates the surface diffuseness as well as the surface energy by around 10%. This could be roughly compensated for by increasing the range parameter a by this relative amount (keeping the value of Ca^3 constant) when using the Thomas-Fermi approximation.

In this paper we have not studied the curvature-energy coefficient nor have we considered asymmetric systems. The curvature energy is probably more sensitive to the quantum effects and it would be interesting to determine this quantity in the Hartree approximation. Such a determination would involve the process of curving the quantum surface and still lies a little ahead. The study of asymmetric systems is rather straightforward; it would provide us with the Hartree values for the nuclear surface-symmetry energy and the neutron-skin thickness. This would give us additional insight into the applicability of the Thomas-Fermi approximation.

The Hartree approximation treats the quantum mechanics in an exact way, within the restriction that the total system be described by a product wave function. The development of the Seyler-Blanchard model in the Hartree approximation may therefore serve as a useful reference for testing and illuminating approximation schemes aiming at improving

the Thomas-Fermi approximation.

As mentioned in the introduction, the Seyler-Blanchard model in the Thomas-Fermi approximation has been used to estimate the thermostatic properties of nuclear matter.[3] It would be relatively easy to perform a similar study within the Hartree approximation. In this way improved results for the temperature dependence of the various surface properties of nuclear matter might be obtained.

All of the aspects mentioned above pertain to isolated nuclear systems. An exciting prospect, brought into focus by the present explosive development in heavy-ion experiments, is the study of the nucleus-nucleus interaction. As will be shown elsewhere, the Seyler-Blanchard model gives rise to a nucleus-nucleus interaction which is expressible in terms of a static interaction potential and a separation-dependent effective mass for the relative motion of the two-nucleus system. For the calculation of these quantities the nuclear surface structure is very important, and an inclusion of the quantum features seems required for an accurate result. With the presented quantum development of the Seyler-Blanchard model this possibility now seems within reach and we are currently investigating this aspect.

A prospect a little further ahead is the development of the model for the treatment of dynamical aspects of a collision between the two nuclear systems. It seems that the Seyler-Blanchard model, in a qualitatively correct way, could produce many of the features characteristic of such a process, and its conceptual simplicity should make it a very useful tool for the investigation of dynamical phenomena associated with a heavy-ion collision process. In this context it should be pointed out that the

Seyler-Blanchard quadratic velocity dependence accounts reasonably well for low-energy phenomena; i.e., when the relative velocity is of the order encountered within a single nucleus. For high-energy nucleus-nucleus collisions, however, considerably larger relative velocities occur and a modification of the repulsive velocity term would be required.

ACKNOWLEDGMENTS

The presented investigation was initiated on the suggestion of W. J. Swiatecki, and his continuing support and encouragement throughout the work is gratefully acknowledged. Furthermore, numerous informative discussions with W. D. Myers as well as his great interest in the project are highly appreciated. Finally, I wish to thank the Lawrence Berkeley Laboratory for the warm hospitality extended to me during the course of this work.

APPENDIX A. SOLUTION OF THE SEMI-INFINITE PROBLEM

In this Appendix we are concerned with the special case of a semi-infinite system. For simplicity, we shall consider only a one-component system; this corresponds to the neutron and proton distributions being identical. The extension to more than one component is straightforward.

A.1. Formulae

We thus consider a semi-infinite system, i.e., a system with translational symmetry in directions parallel to the surface plane. We shall assume that the system is static, i.e., the momentum density distribution is zero everywhere. For such a system the single-particle wave functions may be taken to have the form

$$\psi_i(\vec{r}) = \sqrt{2}\, s(x, p_x, p_\perp) \cdot e^{\frac{i}{\hbar} p_y y} \cdot e^{\frac{i}{\hbar} p_z z} \qquad (A.1)$$

The invariance with respect to translations parallel to the surface implies that the corresponding momenta p_y and p_z are conserved.

Thus we have chosen traveling plane waves in the transversal directions (y and z) and standing waves s (which may be assumed real) in the longitudinal direction (x). The normalization is chosen as one particle per unit volume in the asymptotic bulk of the system ($x \to -\infty$), hence $s \sim \sin$ in that region. The single-particle states are labeled by the momentum quantum numbers in the bulk, p_x and $p_\perp$, the longitudinal and transversal momenta, respectively, where $p_\perp^2 = p_y^2 + p_z^2$. For the semi-infinite system these momenta may take on any values between zero and the

bulk Fermi momentum P_F; hence the index i is a continuous variable and the corresponding summations should be interpreted in terms of momentum-space integrations.

The problem is effectively one-dimensional, and the Schrödinger equation (4.14) for the longitudinal wave functions s now takes the form

$$\left[\frac{d}{dx}\frac{\hbar^2}{2B(x)}\frac{d}{dx} + \frac{p_\perp^2}{2B(x)} + U(x) - E(p_x, p_\perp)\right] s(x, p_x, p_\perp) = 0 \tag{A.2}$$

The effective mass B and the effective potential U are given by:

$$\frac{1}{2B(x)} = \frac{1}{2m}\left(1 + \frac{2m}{b^2} C\mathcal{R}(x)\right)$$
$$U(x) = -C\mathcal{R}(x) + C\mathcal{T}(x) \tag{A.3}$$

Furthermore, the energy eigenvalue E is given by

$$E(p_x, p_\perp) = \frac{p_x^2 + p_\perp^2}{2B_o} + U_o \tag{A.4}$$

where the subscript o refers to the values in the asymptotic bulk region ($x \to -\infty$).

The various densities of interest are given by the following expressions, with prime denoting differentiation,

$$\rho(x) = \sum 2s^2(x) = \frac{t}{h^3}\int^{P_F} 2s(x, p_x, p_\perp)^2 \, d^3\vec{p}$$
$$= 2\pi\frac{t}{h^3}\int_0^{P_F} dp_x \int^{P_F^2 - p_x^2} dp_\perp^2 \, s^2 \tag{A.5}$$

$$\tau(x) = \sum 2(-\hbar^2 ss'' + p_\perp{}^2 s^2)/b^2 = \ldots$$
$$\gamma(x) = \sum 2\left(\frac{1}{2}(-ss'' + s'^2)\hbar^2 + p_\perp{}^2 s^2\right)/b^2 = \ldots \qquad (A.5)$$

For the matter density ρ we have explicitly shown the momentum-space integration involved. The spin-isospin degeneracy is denoted by $t = 4$. As discussed in Subsection 4.3a, only ρ and τ are required for the iteration procedure, while knowledge of γ is necessary for the final establishment of the energy density distribution.

A.2. Numerical Methods

The numerical problems associated with the treatment of the semi-infinite Seyler-Blanchard system are common to a variety of physical contexts. We shall briefly outline here some of the numerical methods employed. Although developed for the present specific problem they can be profited from in other contexts as well.

A.2.1. Exponential Folding

The various potential functions are generated from the density distributions by folding with the Yukawa function. For a semi-infinite system the transversal integration may be performed and leaves an exponential as the folding function in the longitudinal direction.

Some simplifying features are associated with the one-dimensional exponential folding. In order to appreciate this, observe first that the folded functions are of the following form

$$\mathcal{R}\left(\frac{x}{a}\right) = 4\pi a^3 \int_{-\infty}^{\infty} \frac{1}{2} e^{-|x-x'|/a} \rho\left(\frac{x'}{a}\right) d\frac{x'}{a}$$

$$= \mathcal{R}_-\left(\frac{x}{a}\right) + \mathcal{R}_+\left(\frac{x}{a}\right) \tag{A.6}$$

where

$$\mathcal{R}_\pm\left(\frac{x}{a}\right) = \pm 4\pi a^3 e^{\pm x/a} \int_{x/a}^{\pm\infty} \frac{1}{2} e^{\mp x'/a} \rho\left(\frac{x'}{a}\right) d\frac{x'}{a} \tag{A.7}$$

(Similar relations hold for the other folded functions, of course.) In the numerical evaluation of $\mathcal{R}_\pm$ one may benefit from the fact, due to the occurring exponential, that the value of $\mathcal{R}_\pm$ at a certain point is related in a simple way to its value at a neighboring point. This fact reduces the folding from a two-dimensional process to only one dimension.

Another important simplification, due to the exponential, is that closed expressions may be obtained for the first two derivatives of the folded functions. Thus, it is elementary to prove the following relations

$$\frac{d}{d(x/a)} \mathcal{R}\left(\frac{x}{a}\right) = -\mathcal{R}_-\left(\frac{x}{a}\right) + \mathcal{R}_+\left(\frac{x}{a}\right) \tag{A.8}$$

$$\frac{d^2}{d(x/a)^2} \mathcal{R}\left(\frac{x}{a}\right) = \mathcal{R}\left(\frac{x}{a}\right) - 4\pi a^3 \rho\left(\frac{x}{a}\right) \tag{A.9}$$

Hence these derivatives are available without additional computational effort. Moreover, contrary to what would be the case for a numerical differentiation, no further error is introduced. This feature will be exploited in the numerical solution of the Schrödinger equation (Subsection A.2.2).

The densities multiplying the exponential in the integrand have the property of being constant outside a certain region around the nuclear surface ($x = 0$, say). We wish to establish a simple integration scheme which must be accurate in the bulk region since a subtraction is involved

in the calculation of the surface energy. To fulfill these two requirements we have constructed a modified Simpson scheme.

The usual Simpson rule is a three-point integration formula which is exact when the integrand is a parabola. This scheme would yield a constant error in a region with constant density and must be rejected. Instead, we require that the rule yield exact results when the function multiplying the exponential is a parabola. This sophistication leads to a slight modification of the usual Simpson weight coefficients. Thus for an equidistant three-point grid we find the following weights,

$$\begin{aligned} w_o &= 2dx\left[e^{-dx/a}\left(1+\frac{dx}{a}\right) - e^{dx/a}\left(1-\frac{dx}{a}\right)\right]\Big/\left(\frac{dx}{a}\right)^3 \\ w_{\mp} &= \pm dx\left[e^{\pm 2dx/a}\left(1 \mp \frac{1}{2}\,\frac{dx}{a}\right) - 1 \mp \frac{3}{2}\,\frac{dx}{a} - \left(\frac{dx}{a}\right)^2\right]\Big/\left(\frac{dx}{a}\right)^3 \end{aligned} \qquad \text{(A.10)}$$

Here dx is the grid spacing and a is the (known) range of the exponential. The weight w_o pertains to the mid point, $w_{\mp}$ to the left/right endpoint (if a is positive).

The expressions (A.10) for the integration weights may be expanded:

$$\begin{aligned} w_o &= \frac{4}{3}\,dx \sum_{n\geq 0} \frac{3!\,(1+n)}{(2n+3)!}\left(\frac{dx}{a}\right)^{2n} = \frac{4}{3}\,dx\left(1 + \frac{1}{10}\left(\frac{dx}{a}\right)^2 + \frac{1}{280}\left(\frac{dx}{a}\right)^4 + \ldots\right) \\ w_{\mp} &= \frac{1}{3}\,dx \sum_{n\geq 0} \frac{3!\,(1-n)}{(n+3)!}\left(\pm 2\,\frac{dx}{a}\right)^{n} = \frac{1}{3}\,dx\left(1 - \frac{1}{5}\left(\frac{dx}{a}\right)^2 \mp \frac{2}{15}\left(\frac{dx}{a}\right)^3 - \ldots\right) \end{aligned} \qquad \text{(A.11)}$$

The last relations exhibit the modification relative to the standard Simpson rule. Notice that this latter rule emerges in the special case

of a very wide folding function, $a \to \infty$.

In the region of constant density the relative error of the standard Simpson rule is given by $\frac{1}{2dx}(w_- + w_o + w_+) - 1 \approx \frac{1}{60}\left(\frac{dx}{a}\right)^4$. Although locally small, this error would for a large system integrate up to a significant perturbation of the final results.

A.2.2 Differential Equation

The solution of the set of Schrödinger equations constitutes the heaviest numerical burden in solving the problem. The purpose of generating the single-particle wave functions is to construct the various density distributions required for the iteration scheme and for the extraction of the energy density. The general structure of the wave functions in $(x, p_x, p_\perp)$-space is illustrated in figs. 9 and 10. Because, at a given point x, the integrands in the momentum-space integrals exhibit rapid oscillations it is necessary to work with a rather dense grid in momentum space. Consequently the Schrödinger equation must be solved many times for each iteration cycle. And what is more, the occurrence of tiny but numerically significant wiggles in the quantum density distributions demands a large accuracy of each individual wave function. To meet these demands we have developed what appears to be a rather powerful numerical method, based on the standard Taylor-expansion method.

We take advantage of the fact mentioned above that the first few derivatives of the potential functions are well known numerically. Moreover, they are common to all particles in the system and therefore need only be established once for each iteration cycle. The method has the advantage that the limited number of derivatives available may

be compensated by an appropriately shorter step size.

The second order Schrödinger equation $\frac{d}{dx}\,\frac{1}{a}\,\frac{d}{dx}\,f = bf$ may be cast into the form of two coupled first-order equations. This leads to a system of the following form,

$$\frac{d}{dx}\begin{pmatrix} f \\ g \end{pmatrix} = \mathbb{D}\begin{pmatrix} f \\ g \end{pmatrix}, \qquad \mathbb{D} = \begin{pmatrix} o & a \\ b & o \end{pmatrix} \tag{A.12}$$

where the auxiliary function g is given by $g = \frac{1}{a}\,\frac{d}{dx}f$. By successive differentiation of this couple of equations it is possible to express the derivatives of f and g solely in terms of f and g themselves and derivatives of the potential functions a and b which form the coefficient matrix $\mathbb{D}$. Knowing the derivatives of f and g at a certain point we may obtain the functions at a neighboring point by employing the Taylor expansion formula:

$$f(x + dx) = f(x) + f'(x)dx + \frac{1}{2}\,f''(x)dx^2 + ... \tag{A.13}$$

The accuracy of the generated solution may be checked in a simple and confident way by shortening the step size dx.

Far outside the system, where the nuclear potential is zero, the wave functions are decaying exponentials. This provides us with a set of initial conditions for the ratio f/g. With an arbitrary normalization factor the equations may then be integrated through the interesting region until the bulk region is reached. Here again the potential is constant and the wave functions are trigonometric functions. This fact enables us to determine from a bulk set of f and g the true normalization factor.

The Taylor-expansion method yields the wave functions in a fixed x grid. This is an important advantage relative to possible variable-grid methods because afterwards we need to sum up all the solutions at a certain spatial point to obtain the value of the desired density distributions. Thus any numerical interpolation is avoided in the employed method.

It may be noted that in the general case of a non-static system, the described method still applies. The effective momentum operator is now a combination of a differentiation and a multiplication operator (4.12). But this merely introduces two diagonal terms in the coefficient matrix **D** in addition to the two off-diagonal terms already present. Consequently the whole procedure still carries through essentially unchanged.

Finally, it should be pointed out that the subsequent calculation of the various density distributions ρ, τ, γ, ... does not involve any numerical differentiation because we already have available very accurate values from the solution process for the derivatives of the wave functions. This advantage increases further the numerical precision of the results.

A.2.3. Momentum-Space Integration

The momentum-space integration poses a delicate numerical problem because of the rapid oscillation of the integrands. Away from the surface the wave functions vary approximately like $\sin(p_x x + \eta(p_x, p_\perp))$ where η is some phase shift. Hence the integrand varies more and more rapidly the deeper inside the system we are. This is illustrated in fig. 9. Furthermore, the endpoints $p_x = 0$ and $p_x = P_F$ pose special problems, the first one because we cannot calculate for vanishing momentum, and the second one because the transversal-momentum integration becomes relatively

unreliable.

We shall not go into any details here, but a closer analysis reveals that in these two situations a Simpson scheme tends to be exact. Furthermore, the variation with $p_\perp^2$ is rather moderate, as may be seen from fig. 10 hence a simple integration scheme is sufficient for the transversal-momentum integration. We have therefore chosen to use the Simpson scheme for the p_x as well as the $p_\perp^2$ integration. Although this may seem crude, the fact that the fine density ripples deep inside the system are produced accurately constitutes a very thorough check of the whole momentum-space integration.

The various parameters governing the accuracy of the numerical procedures were varied in order to ensure reliable results. This led to the following conclusions.

For the Taylor-integration of the Schrödinger equation it was found that a step size of 0.1a was sufficient when potential derivatives up to third order were included. For the subsequently momentum-space integration it was found that around 8 grid points for the transverse-momentum integration and around 8 grid points per hump for the p_x integration were satisfactory. Furthermore, it was determined that the surface integrals could be cut off at a depth of around 20a. The iterative scheme showed a good convergence and after five iterations no further significant improvement could be obtained.

It should be pointed out that substantial increases (doubling) in any of these requirements left the accepted results unchanged within the allowed tolerance.

REFERENCES

1) R. G. Seyler and G. H. Blanchard, Phys. Rev. 124 (1961) 227; 131 (1963) 355

2) W. D. Myers and W. J. Swiatecki, Ann. Phys. 55 (1969) 395

3) W. A. Küpper, G. Wegmann and E. Hilf, "Thermostatic Properties of Nuclear Matter", Lawrence Berkeley Laboratory Preprint LBL-642 (1974)

4) J. Randrup, W. J. Swiatecki and C. F. Tsang, "Proximity Forces", Lawrence Berkeley Laboratory Preprint LBL-3603 (1974), to be published

5) J. Blocki, private communication, July 1974

6) E. Hilf, private communication, August 1974

7) A. Bohr and B. R. Mottelson, "Nuclear Strucutre", Vol. 1, Benjamin, 1969

8) M. A. Thorpe and D. J. Thouless, Nucl. Phys. A156 (1970) 225

9) G. Süssmann, "Description of the Nuclear Surface by Moments", Lawrence Berkeley Laboratory Reprint LBL-1615 (1973)

10) H. Gräf, private communication, November 1974

11) W. J. Swiatecki, Proc. Phys. Soc. A68 (1955) 285

12) H. S. Köhler, Nucl. Phys. A139 (1969) 353

Table 1. Various characteristic surface quantities as obtained within the Thomas-Fermi and Hartree approximations. The quantities are: 10-90% surface diffuseness of matter density, the similar diffuseness based on the second surface moment, the kinetic part of the surface-energy coefficient, the interaction part, the total surface-energy coefficient, the 10-90% diffuseness of the mass function, and the 10-90% diffuseness of the potential. The last column shows the relative change (in percent) in going from the Thomas-Fermi to the Hartree approximation.

Quantity	Thomas-Fermi	Hartree	Change [%]
t_{10-90} [a]	3.17	3.51	10.7
b [a]	1.39	1.47	5.8
a_s^{kin} [MeV]	-16.22	-16.88	4.1
a_s^{int} [MeV]	34.79	37.38	7.4
a_s [MeV]	18.56	20.51	10.5
t^B_{10-90} [a]	4.30	4.95	15.1
t^U_{10-90} [a]	4.55	5.10	12.1

FIGURE CAPTIONS

Fig. 1. Matter density distributions in units of the bulk density ρ_o. The smooth curve is the Thomas-Fermi result and the oscillating curve is the Hartree result. The dashed density corresponds to an infinite wall located such that the wiggles are in phase with the Hartree wiggles deep inside the system. The scale has been enlarged by a factor of ten for $x < -7a$ in order to exhibit the density wiggles.

Fig. 2. Doubly logarithmic plot of the relative amplitude of the Hartree density wiggles as function of the depth. The straight lines correspond to the inverse square dependence pertaining to an infinite wall while the curved line joins the actual results, from the third to the seventeenth undulation. The vertical scale extends from 0.01 to 0.0005.

Fig. 3. Kinetic-energy density distributions in units of $\frac{b^2}{2m}\rho_o$. The full curve is the Hartree result and the dashed curve the Thomas-Fermi result.

Fig. 4. Various kinetic density distributions in units of $\frac{b^2}{2m}\rho_o$. The curve labeled τ represents the standard kinetic energy displayed in fig. 3 while κ represents the "velocity squared" density. The average of these two densities is γ, the density that enters in the Seyler-Blanchard energy expression.

Fig. 5. Surface-energy density distributions in units of MeV/a^3. Full line: Hartree, dashed line: Thomas-Fermi.

Fig. 6. Kinetic and interaction parts of the surface-energy density distributions displayed in fig. 5.

Fig. 7. The effective mass function B in units of the nucleon mass m, and the effective static potential U in units of $b^2/2m$. Full line: Hartree, dashed line: Thomas-Fermi. The position of the 10% and 90% points as well as the asymptotic values are indicated.

Fig. 8. The potentials U^a (full line) and U^b (dashed line) corresponding to the two illustrations in Section 3. The commutator contribution δU is shown on a ten times enlarged scale.

Fig. 9. Schematic structure of the longitudinal wave function s as function of x and p_x for fixed transversal momentum $p_\perp = 0$. The center of the figure is an x-p_x diagram showing the nodal structure of s; also the location of the turning points as given by the condition $U = E$ is indicated. To the left of this diagram is shown an end view corresponding to a large depth; the wave function exhibits a rapid oscillation as function of p_x. To the right is a similar end view from the tail region outside the system; the wave function increases exponentially with p_x. Above the nodal diagram is shown the wave function for the most energetic particle $p_x = P_F$ and below the wave function for a low-momentum particle $p_x << P_F$.

Fig. 10. Absolute value of the wave function s as function of p_x for fixed $x = -14.3a$ and two extreme values of $p_\perp^2$: $p_\perp^2 = 0$ (full line) and $p_\perp^2 = P_F^2 - p_x^2$ (dashed line).

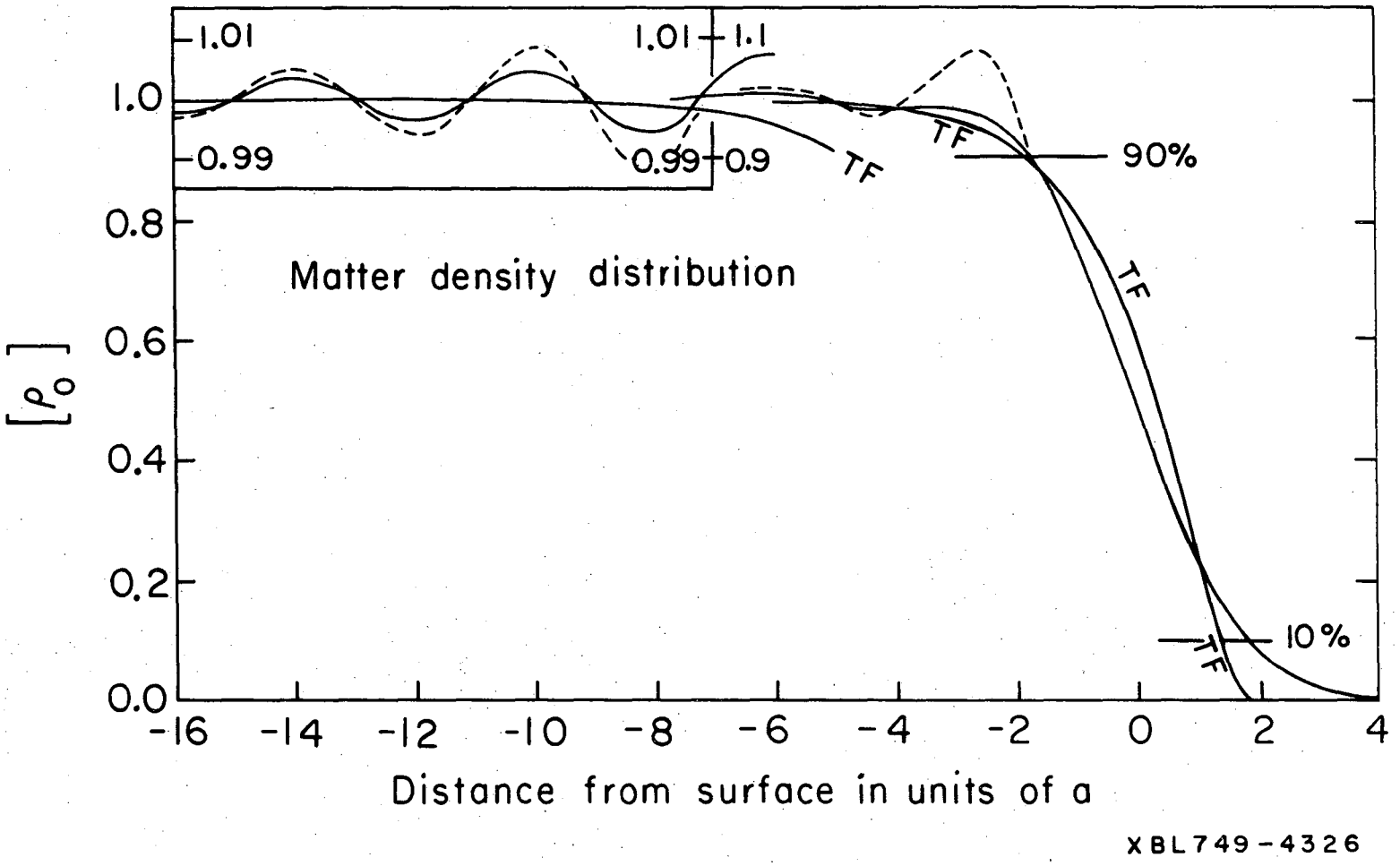
1.01
1.01
1.1
1.0
0.99
0.99
0.9
TF
TF
90%
0.8
Matter density distribution
TF
$[\rho_0]$
0.6
0.4
0.2
10%
TF
0.0
-16
-14
-12
-10
-8
-6
-4
-2
0
2
4
Distance from surface in units of a
XBL749-4326

Figure 1

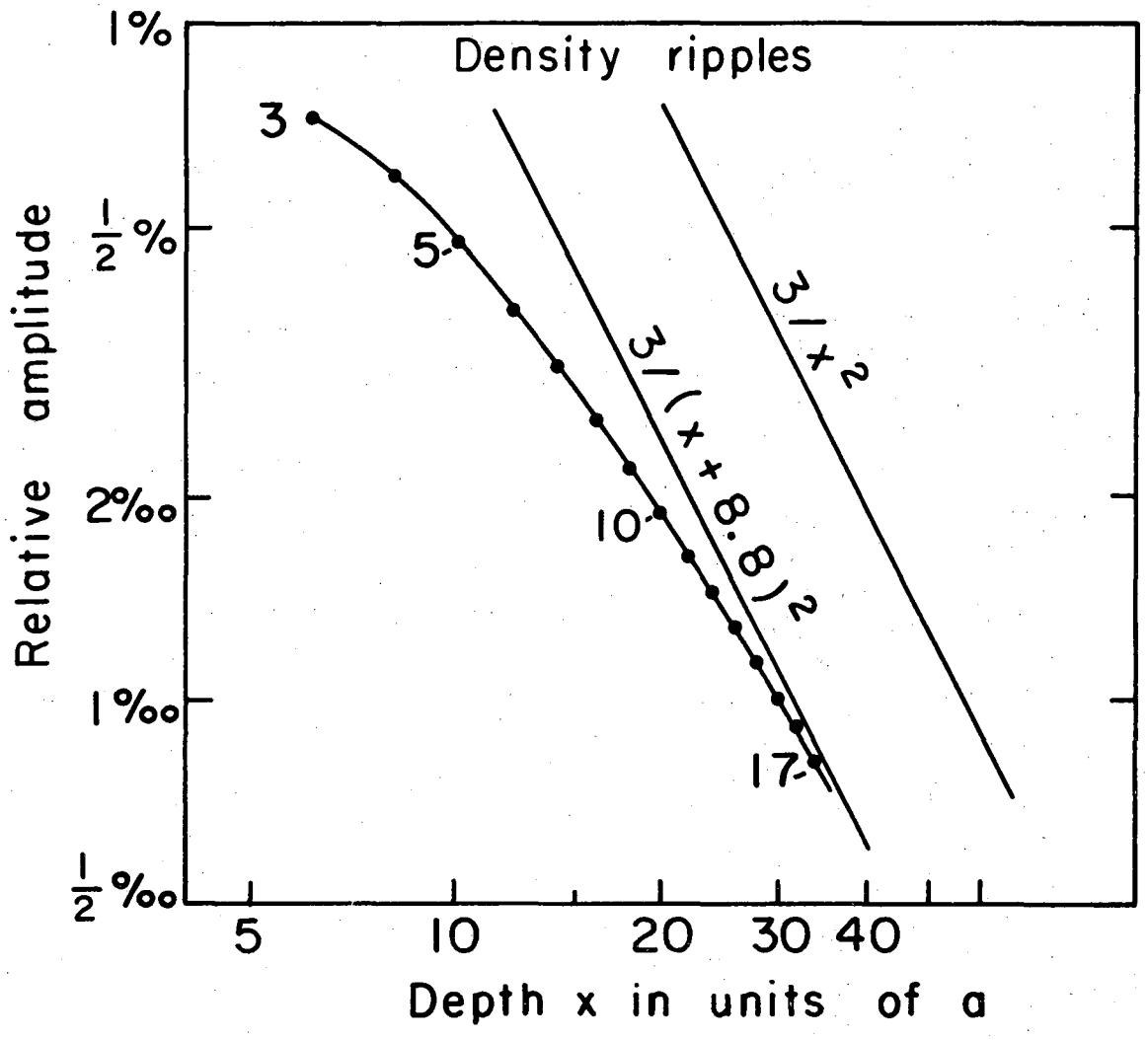

XBL749-4319

Figure 2

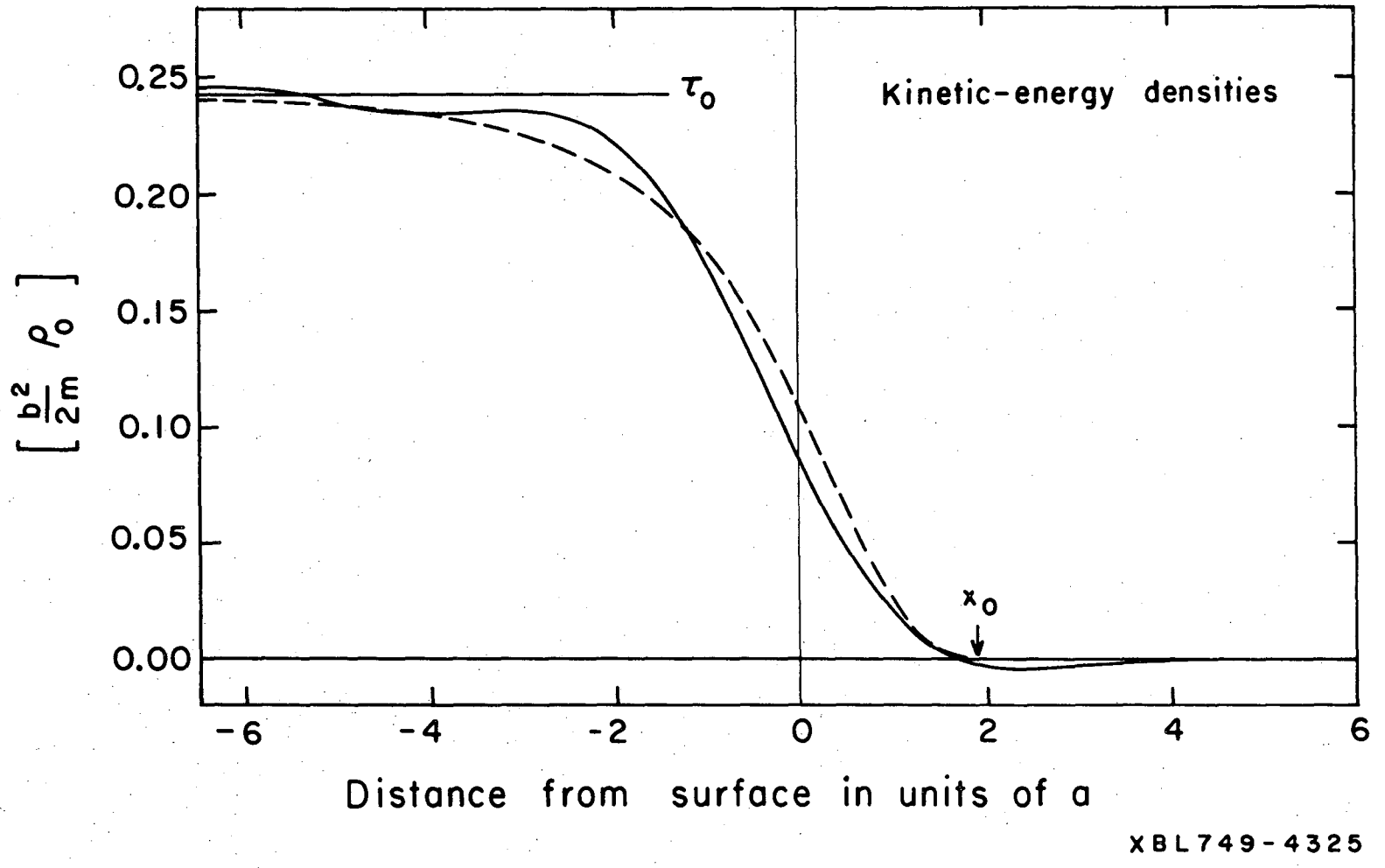
Kinetic-energy densities
τ_0
x_0
0.25
0.20
0.15
0.10
0.05
0.00
$\left[\frac{b^2}{2m}\rho_0\right]$
-6
-4
-2
0
2
4
6
Distance from surface in units of a
XBL749-4325

Figure 3

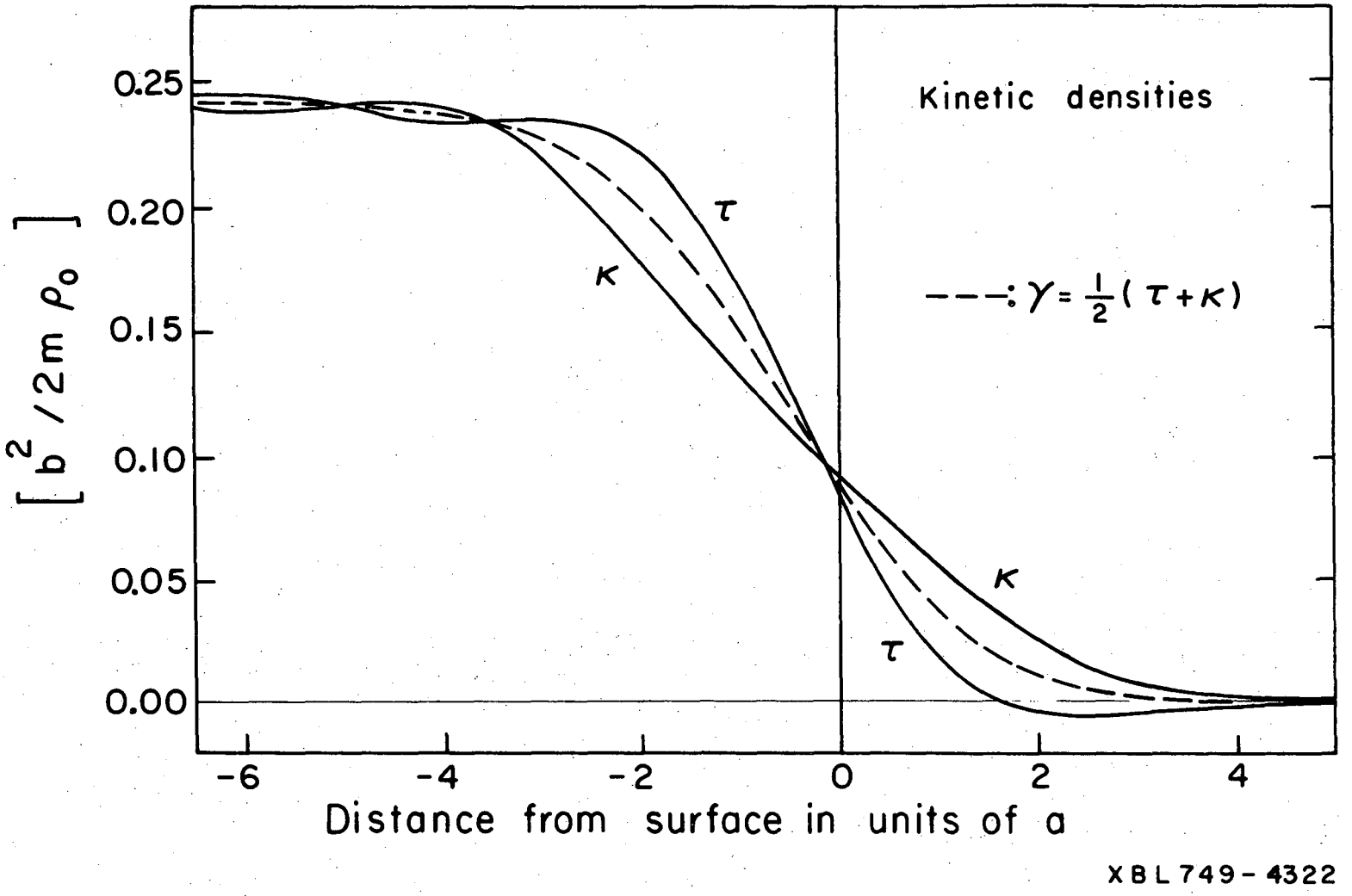
Kinetic densities
---: $\gamma = \frac{1}{2}(\tau + \kappa)$
τ
κ
κ
τ
$[\hbar^2/2m\rho_0]$
0.25
0.20
0.15
0.10
0.05
0.00
-6
-4
-2
0
2
4
Distance from surface in units of a
XBL749-4322

Figure 4

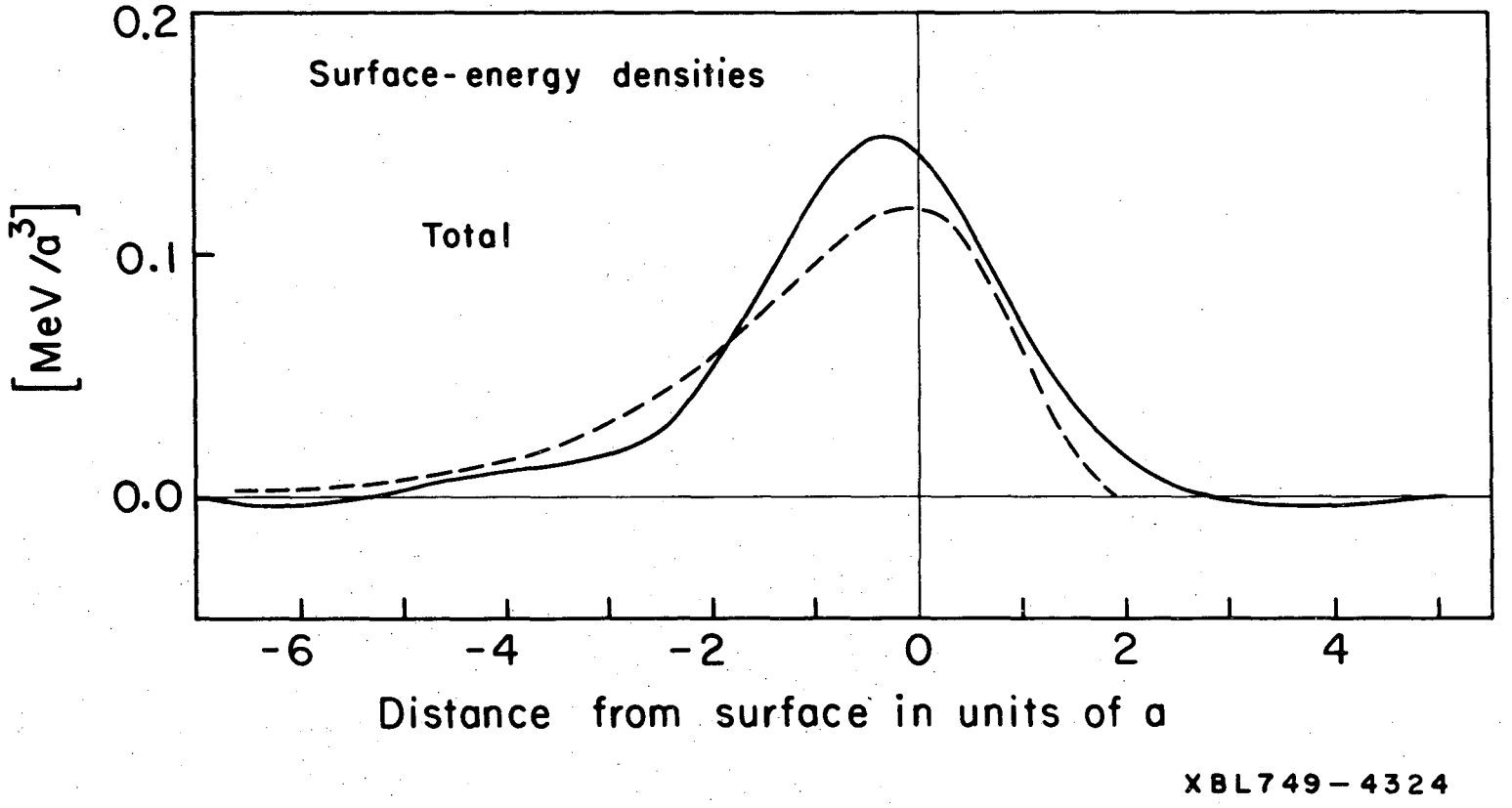
Surface-energy densities
Total
0.2
0.1
0.0
[MeV/a^3]
-6
-4
-2
0
2
4
Distance from surface in units of a
XBL749-4324

Figure 5

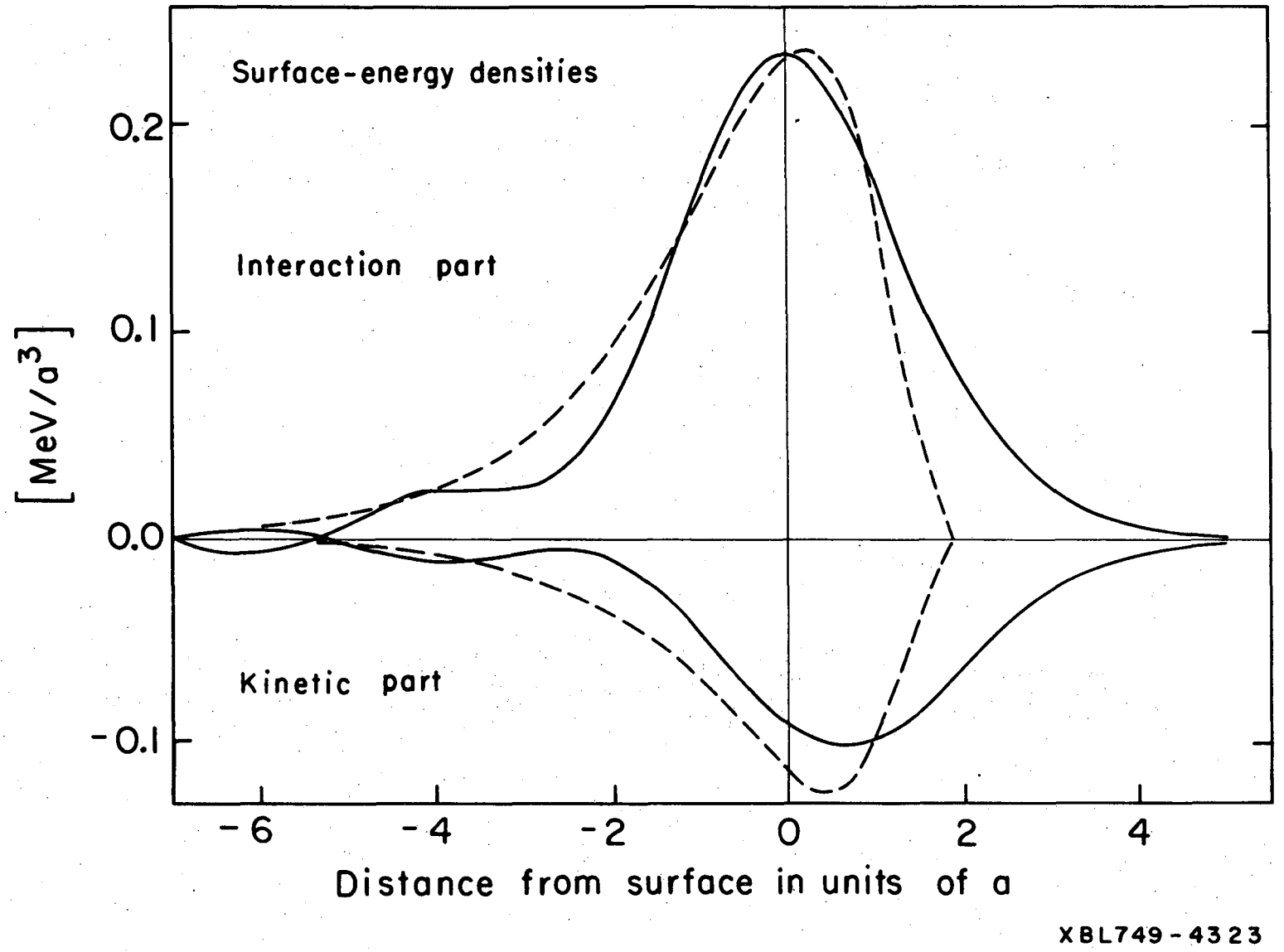
Surface-energy densities
Interaction part
Kinetic part
0.2
0.1
0.0
-0.1
[MeV/a³]
-6
-4
-2
0
2
4
Distance from surface in units of a
XBL749-4323

Figure 6

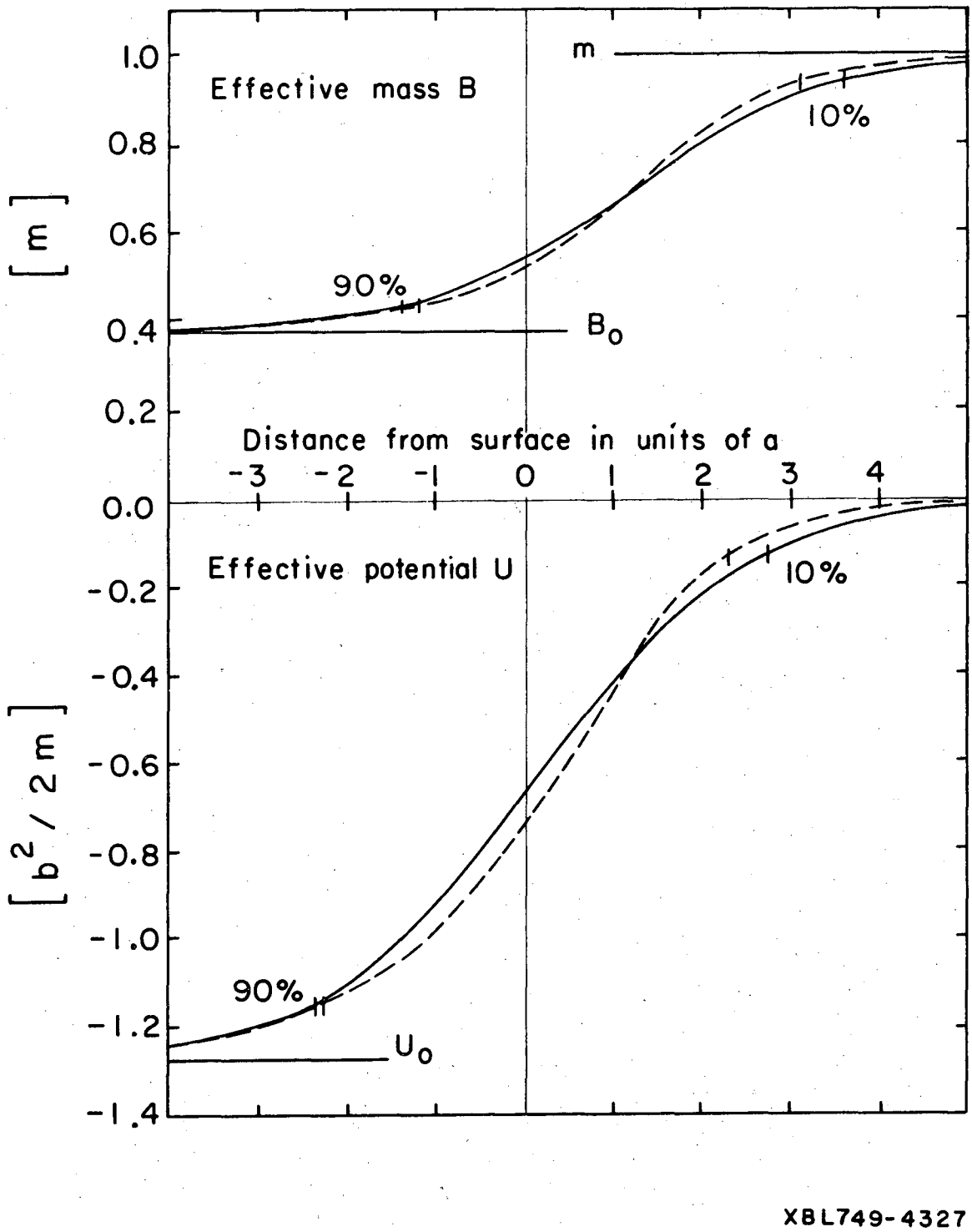
Effective mass B
m
10%
90%
B_0
Distance from surface in units of a
-3 -2 -1 0 1 2 3 4
Effective potential U
10%
90%
U_0
[m]
$[b^2/2m]$
1.0
0.8
0.6
0.4
0.2
0.0
-0.2
-0.4
-0.6
-0.8
-1.0
-1.2
-1.4
XBL749-4327

Figure 7

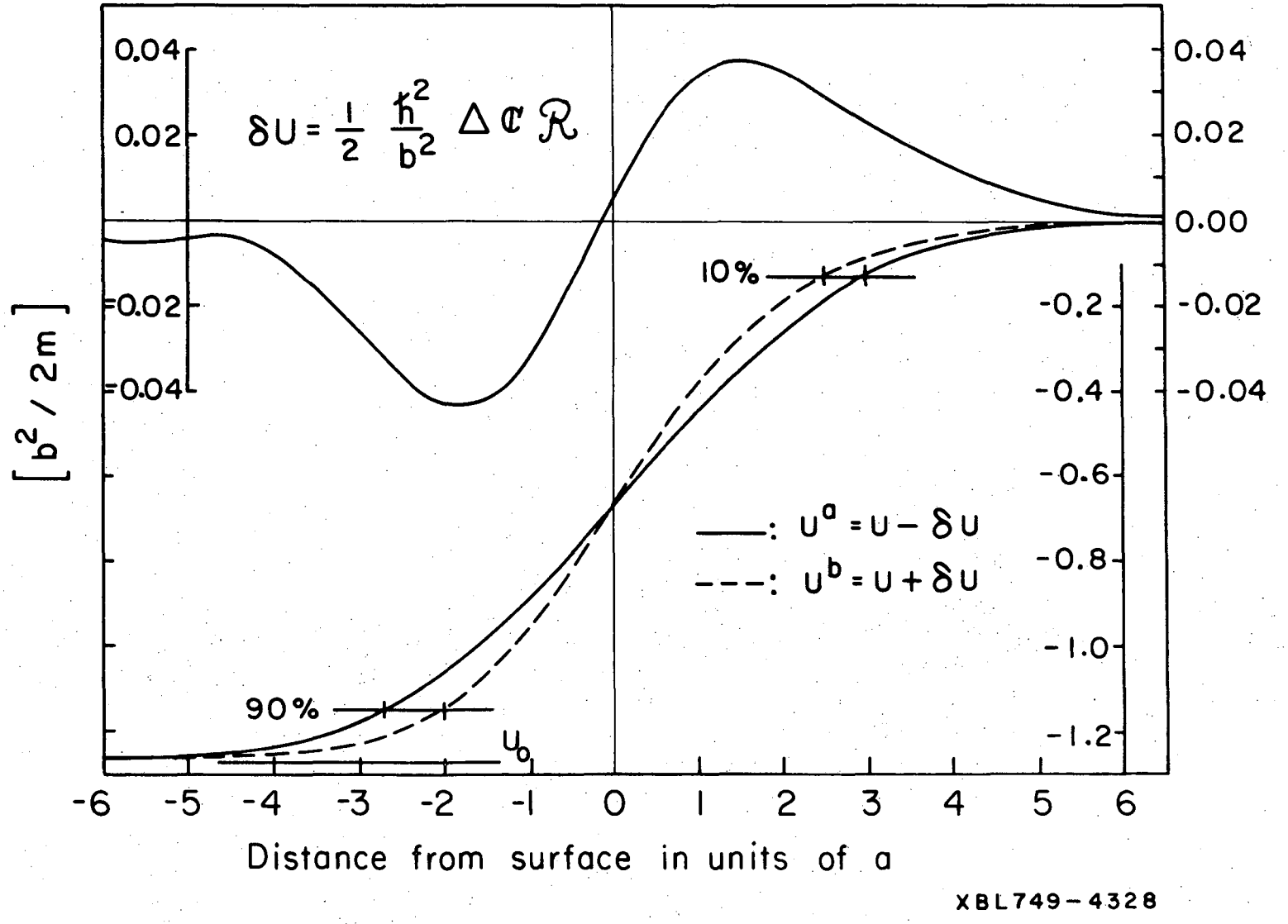
0.04
0.02
$\delta U = \frac{1}{2} \frac{\hbar^2}{b^2} \Delta \mathcal{C} \mathcal{R}$
0.04
0.02
0.00
-0.02
-0.04
$[b^2 / 2m]$
10%
90%
U_0
-0.2
-0.4
-0.6
-0.8
-1.0
-1.2
——: $U^a = U - \delta U$
– – –: $U^b = U + \delta U$
-6 -5 -4 -3 -2 -1 0 1 2 3 4 5 6
Distance from surface in units of a
XBL749-4328

Figure 8

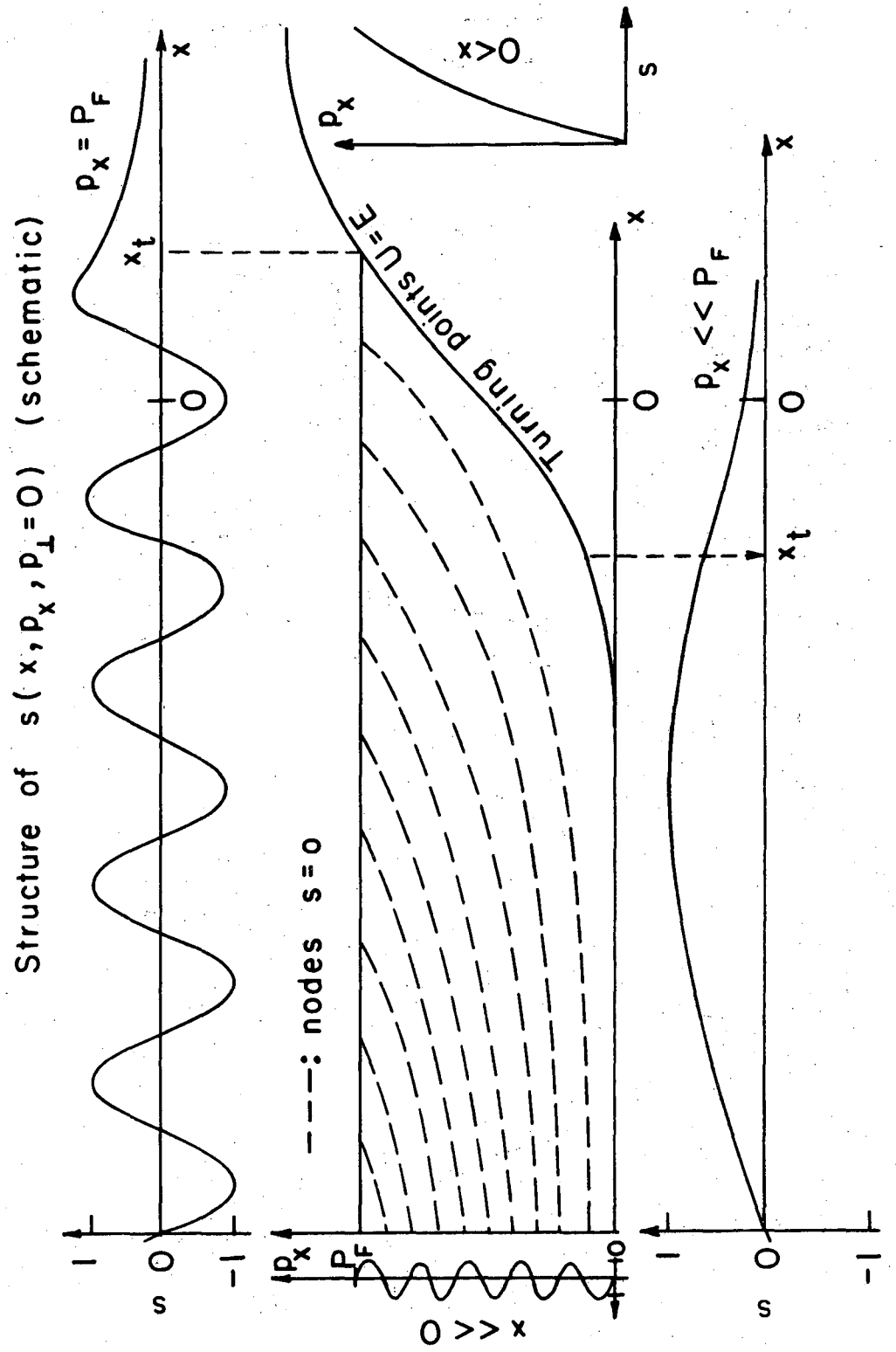
Structure of s(x, p_x, $p_\perp$=0) (schematic)
$p_x = P_F$
x_t
x
0
1
0
-1
s
---: nodes s = 0
Turning points U=E
p_x
P_F
0
x << 0
x>0
p_x
s
$p_x << P_F$
x_t
XBL 749-4321

Figure 9

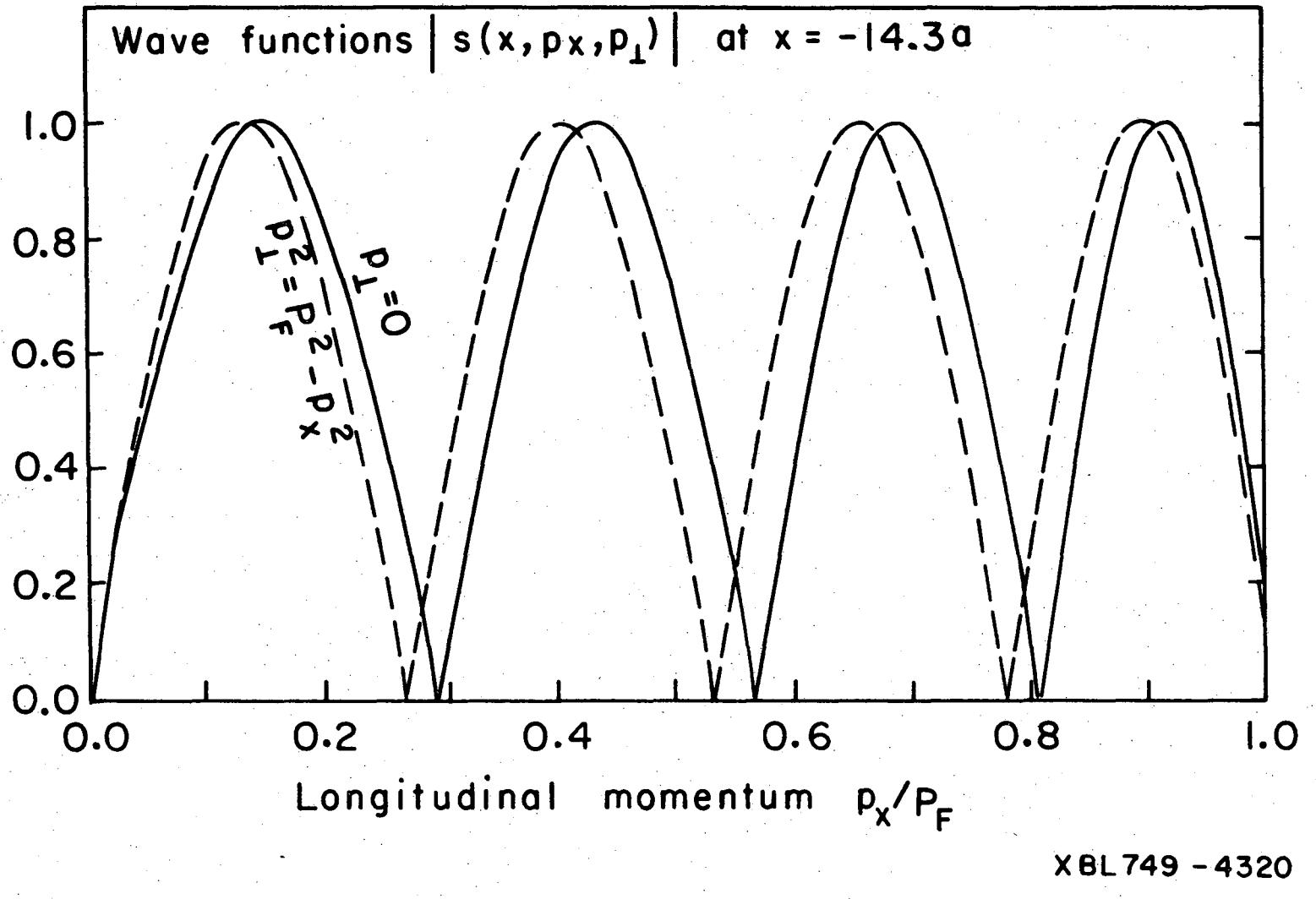
Wave functions | s(x, px, p⊥) | at x = -14.3a
1.0
0.8
0.6
0.4
0.2
0.0
0.0
0.2
0.4
0.6
0.8
1.0
p⊥=0
p⊥²=pF²-px²
Longitudinal momentum px/pF
XBL749-4320

Figure 10

TECHNICAL INFORMATION DIVISION
LAWRENCE BERKELEY LABORATORY
UNIVERSITY OF CALIFORNIA
BERKELEY, CALIFORNIA 94720